MOLECULAR DYNAMICS SIMULATION STUDY OF SILICON NANOTUBES

by

Mustafa Selçuk Yaşar

A Thesis Submitted to the
Graduate School of Engineering
in Partial Fulfillment of the Requirements for
the Degree of

Master of Science

in

Physics

Koç University

August, 2008

Koç University

Graduate School of Sciences and Engineering

This is to certify that I have examined this copy of a master's thesis by

Mustafa Selçuk Yaşar

and have found that it is complete and satisfactory in all respects,
and that any and all revisions required by the final
examining committee have been made.

Committee Members:

_____

Prof. Tekin Dereli

_____

Prof. Gülay Dereli

_____

Assist. Prof. Alkan Kabakçıoğlu

Date: _____

To my sister

ABSTRACT

Since carbon and silicon lie in the same group of elements in the periodic table and have similar electronic configurations, the possibility of having silicon nanotubes similar to the conventional carbon nanotubes have attracted much recent attention. Single walled silicon hexagonal nanotubes (hNTs) should be formed by rolling-up graphene-like silicon sheets. In recent literature, many correlative theoretical predictions have been performed on such silicon nanotubes.

In this thesis work, a semi-empirical tight-binding molecular dynamics (TBMD) technique is employed in the simulation studies of single walled silicon hNTs. Appropriate tight-binding pair potential parameters are obtained by fitting the results of *ab initio* calculations. We optimized the silicon hNTs having the same predicted total energy values reported in the literature. The effects of chirality and diameter on the energetics, strain energies, and electronic density of states of single walled silicon hNTs have been studied on several types of armchair and zigzag nanotubes. We present the results of our TBMD simulations and discuss about the possible stability of silicon hNTs.

ÖZETÇE

Karbon ve silikon elementleri periyodik tabloda aynı grupta bulundukları ve benzer elektronik konfigürasyonlara sahip oldukları için bilinen karbon nanotüpler gibi silikon nanotüplerin de bulunması olasılığı son zamanlarda büyük ilgi toplamaktadır. Tek duvarlı hekzagonal silikon nanotüpler (hSiNT) grafin benzeri silikon yüzeylerin yuvarlanmasıyla oluşturulabilirler. Literatürde bulunan kuramsal öngörülerin pek çoğu bu tür silikon nanotüpler üstünedir.

Bu tezde tek duvarlı hekzagonal silikon nanotüplerin simulasyonu yarı-ampirik sıkı-bağ moleküler dinamik (TBMD) teknikleri kullanılarak yapılmaktadır. Uygun sıkı-bağ çift potansiyel parametreleri *ab initio* hesaplama sonuçlarına çakıştırılarak belirlenmiştir. Hekzagonal silikon nanotüpler için bu değerler literatürde verilen toplam enerji değerlerini verecek şekilde optimuma getirilmiştir. Farklı simetrik yapıdaki tek duvarlı hSiNT'ler için çalışmalar yapılarak kiralite ve yarıçapın enerji, germe enerjisi ve elektronik durum yoğunluğu üzerine etkisine bakılmıştır. TBMD simulasyon sonuçlarımız verilmiş ve hSiNT'lerin kararlı olup olamayacakları tartışılmıştır.

ACKNOWLEDGMENTS

First and foremost, I would like to thank my advisor, Prof. Tekin Dereli, who provided the right balance of suggestions, criticism, and freedom in my studies. Tekin Dereli consistently gave me good advice, in both personal and professional terms during my study at Koç University, Istanbul.

Prof. Gülay Dereli gave me much needed help when I was studying on my thesis. I am grateful to Prof. Gülay Dereli for her support and guidance. I also thank the members of her group (Carbon Nanotube Simulation Laboratory at Yıldız Technical University, Istanbul) for discussions.

I thank my family for their role in my education throughout the years.

Finally I would like to thank the members of my thesis committee for examining (and hopefully approving) this thesis.

TABLE OF CONTENTS

LIST OF FIGURES

NOMENCLATURE

SW	Single-Wall
NT	Nanotube
SWCNT	Single-Wall Carbon Nanotube
SWSiNT	Single-Wall Silicon Nanotube
h-NT	Hexagonal Nanotube
g-NT	Gear-like Nanotube
TB	Tight-Binding
MD	Molecular Dynamics

Chapter 1

INTRODUCTION

Since the discovery of single wall carbon nanotubes (SWCNTs) more than a decade ago, other types of nanotubes have been predicted. Ideal SWCNTs are considered as graphene sheets rolled up to make hollow cylinders, unique one dimensional nanostructures with their exceptional mechanical and electronic properties. For example, SWCNTs can be metal or semiconductor depending on the diameters and chiralities [1]. In addition, they have a number of remarkable mechanical properties with regard to their flexibility, their ability to withstand twisting distortions, and their ability to withstand compression without fracture. For instance, SWCNTs can be bent around small circles or about sharp bends without breaking [1].

Silicon has been one of the most important materials for electronic devices and silicon-based materials have been the focus of extensive research. Furthermore, in the field of nanotechnology, new forms of stable silicon in the nano-dimension are required to sustain the current silicon based technology. Due to their apparent compatibility with the silicon-based micro-electronics and the prospects of becoming the most versatile building materials for nano-electronic devices, a great interest with the low dimensional silicon nano-structures had been aroused in nanotechnology [2]. Moreover, due to the fact that silicon and carbon are in the same column of the periodic table and own four valance electrons, silicon nanotubes similar to the conventional SWCNTs attracted much attention.

Given the similar electronic configurations of silicon and carbon atoms and the technological importance of silicon, silicon nanotubes have been the subject of many theoretical studies, even if only at a speculative level. Many groups have predicted

the possible stability of silicon nanotubes. However it should be noted that although silicon atoms have similar electronic structure with carbon atoms, their behavior in forming chemical bonds is quite different [1]. For example, sp^2 hybridization is stable in carbon and it can easily form two dimensional planar structures and nanotubes composed of only sp^2 bonds. However, silicon has been well known as just being in the form of diamond. Due to the lack of sp^2 hybridization in silicon, we might conclude that silicon cannot form local planar structures and nanotubes. But nevertheless even though the difficulties in having an sp^2 structure for silicon, many theoretical studies on silicon nanotubes have been done using atomic simulation techniques in recent years [2-14].

Theoretical studies have played an important role in the development of the science surrounding carbon nanotubes. For example, even before any experimental observations, the electronic properties of SWCNTs have been predicted. These predictions that the conductivity of SWCNTs depend on the diameter and the chirality have been confirmed experimentally. In the literature, two types of silicon nanotubes are studied using *ab initio* calculations: SW silicon hexagonal nanotubes (h-NTs) [2,4,5,7-13] and SW silicon gear-like nanotubes (g-NTs) [5-7]. Like SWCNTs, the analogous SW silicon hexagonal nanotubes (h-NTs) are formed by rolling-up the graphene-like silicon sheets. In addition, gear-like nanotubes (g-NTs) are formed by rolling the (111) sheet of the diamond structure.

Unlike SWCNTs, the analogous silicon h-NTs, based on rolling-up graphene-like sheets, are yet to be made. Recently, the synthesis of silicon nanotubes has been demonstrated by various groups, each using a different growth process. However, the structural properties of the fabricated silicon nanotubes are different from those of CNTs. The thickness of ideal SWCNTs are less than one nanometer, i.e. a few Angstroms. However, the thickness of the shells of the fabricated silicon nanotubes are more than several nanometers with the shells consisting of crystalline silicon [15]. Even though ideal SW silicon h-NTs have never been observed experimentally, theoretical studies on such silicon nanotubes have been performed.

Most of the simulation studies revealed how unfavorable the SiNT structure is with respect to the most stable silicon diamond structure. Fagan *et al* [4] [11] investigated the stability of SWSiNTs with the structures of SWCNTs, namely single wall silicon h-NTs. They have shown that there is a significant cost to produce graphenelike sheets of silicon, but once they are formed, the cost to produce a SWSiNT by curving the graphenelike sheet into a cylinder is of the same order of the equivalent cost in carbon. In addition, they established theoretical similarities between SWCNTs and silicon h-NTs. Their results revealed that the electronic properties of silicon h-NTs are similar to those of SWCNTs; depending on the diameter and chirality, they may exhibit metallic or semiconductor behavior. Çıracı *et al* [10] have also shown that zigzag SW h-NTs are metallic for $6 \leq n \leq 11$ and a band gap starts to open for $n \geq 12$. The strain energies of zigzag and armchair silicon h-NT structures have also been obtained by Barnard *et al* [9]. The results indicate the dependence of the strain energies on both diameter and chirality. They have found that the strain energy for a zigzag $(n, 0)$ h-NT is lower than the stain energy of an armchair nanotube (n, n), for the same value of n. Yang *et al* [5] studied SW silicon h-NTs and g-NTs with different diameters and chiralities. They performed the calculations of total energies and electronic properties of silicon h-NTs and g-NTs using VASP (Vienna Ab initio Simulation Package).

In the present work, we apply TB models, so successfully used to study mechanical and electronic properties of SWCNTs [18-22], to the silicon h-NTs that have sp^2 hybridization. The stability, mechanical and electronic properties SWCNTs have been well explained by Dereli *et al* [18-22] using the TBMD model. In this thesis, silicon h-NTs are built in analogy with SWCNTs. Silicon h-NTs are constructed by replacing the carbon atoms. Several groups have performed geometrical optimization of such nanotubes and reported average distances between nearest silicon atoms in SW silicon h-NTs with different chiralities. The nearest neighbor distances for the SW silicon h-NTs are found by Çıracı *et al* [10] around $2.22\mathring{A}$. In addition, Fagan *et al* [4] [11] have found that the nearest neighbor distances for the (6,6) and (10,0)

nanotubes are around 2.245$\mathring{A}$.

In addition, the TBMD model that we have employed in our studies is almost the same with the TBMD model used by Dereli *et al* [18-22] in their simulation studies of SWCNTs. We used the TBMD method adopted from L. Colombo [25]. First we formed graphenelike silicon sheet with the *ab initio* [5] calculated nearest neighbor separation 2.245$\mathring{A}$. Then we bent the graphenelike silicon sheet and periodic boundary conditions were imposed in axial direction along the tube and free boundary conditions in the radial direction. All the simulations presented in this work are carried out in the canonical (NVT) ensemble. The Newtonian equations of motion are integrated using the velocity Verlet algorithm. Using the same techniques, an isolated SWCNT were simulated effectively by Dereli *et al*.

The basic idea of the TBMD technique is the representation of one-electron wave function as a linear combination of localized atomic orbitals, assuming a minimal basis set and short ranged interactions. The use of TB method coupled with MD plays the role of a bridge between model potential and first principle simulations [25], [26]. The TBMD model that we have employed in our simulation studies has been mainly developed at the semi-empirical level, i.e. TB Hamiltonian matrix elements are considered as parameters to be fitted. A number of approximations are further introduced in order to reduce the overall computational workload as much as possible. The basic theory of TB formalism and key features of TBMD technique will be discussed in more detail in Chapter 2 and Chapter 3. The TB hopping integrals, scaling functions and repulsive potential are determined by fitting a suitable database obtained either from experiments or first principles calculations. The TB functional forms suggested by Goodwin *et al* [27] for the hopping parameters and pairwise potential are introduced in the third chapter.

TB parameters for carbon and silicon can be found in the literature. In our studies we have adopted TB parameters for carbon and silicon suggested by Xu *et al* [23] and Kwon *et al* [24], respectively. Both Xu *et al* and Kwon *et al* developed TB interatomic potentials in which they adopted the functional forms given by Goodwin *et al* [27]

for the dependence of the TB hopping parameters and the pairwise potential on the interatomic separation. It is clear that the usefulness of a TB model in describing a wide variety of structures is closely related to its transferability. For example, the set of TB parameters for carbon suggested by Xu *et al* [23] is transferable to the graphene structure. Therefore Dereli *et al* adopted these parameters in their TBMD simulation studies of SWCNTs and successfully optimized nanotubes. In other words, the TB model presented by Xu *et al* for carbon is transferable to the graphene structure and the results that Dereli *et al* have obtained by adopting this model in TBMD simulation studies of SW Carbon NTs are in good agreement with those obtained from ab initio calculations.

On the other hand, the TB model for silicon presented by Kwon *et al* [24] accurately describes the behavior of silicon in crystalline phases. However, their model does not give the energy curve of the hexagonal silicon graphenelike sheets. We adopted from their model only the free parameters contained in the scaling functions for the TB hopping integrals. Then for the set of parameters that we have adopted from Kwon *et al*, the energies of the silicon h-NTs are fitted to the *ab initio* results with a nonlinear least-squares fitting routine to extract values for the two-body functional parameters. Our basic strategy to derive the set of TB parameters for silicon graphenelike structures is discussed extensively in Chapter 3. Once we have determined the TB parameters for the silicon graphenelike structures, any parameter is once-for-all-fixed. No further adjustments of them have been operated during the simulation. At each MD step the total force on each of the nuclei to move atoms is computed. The contributions to the total force is discussed extensively in this thesis, i.e. Hellmann-Feynman contribution and the contribution due to the repulsive potential.

Finally in order to investigate the effects of chirality and diameter on the energetics, structural, and electronic properties of single wall SW silicon h-NTs, the developed TBMD simulation method is employed in this thesis. We explored the possibility of the existence of silicon h-NTs via our semi-empirical TBMD simulation

method. In this thesis we also examined the diameter and chirality dependence of the strain energies. We compared our results with the results obtained by the *ab initio* calculations [4] [5] [5] [9] [10] [11].

This thesis is organized into five chapters. In the remaining part of this chapter, we give a brief summary of molecular simulation techniques and introduce the hybridization in carbon and silicon atoms. We define the geometry of SWCNTs and the analogous SW silicon h-NTs. In the Chapter 2 of this thesis, an overview of MD simulation methods, an introduction to the molecular dynamics and the basic theory of the tight binding formalism are presented. The TB model coupled with MD and a detailed explanation of the computational techniques employed in this thesis is presented in Chapter 3. In addition, appropriate tight-binding pair potential parameters for silicon h-NTs that we have obtained by fitting the results of *ab initio* calculations are introduced in this chapter. The results of our calculations have been presented in Chapter 4. We investigated the effects of chirality and diameter on the energetics, structural, and electronic properties of SW silicon h-NTs and commented on the structural stability and possibility of the existence of SW silicon h-NTs. The *ab initio* structural and electronic properties of hypothetical h-NTs are given and compared with the results of our calculations. Finally, in Chapter 5, the conclusion is found.

1.1 Molecular Simulations

The basic concept of a molecular dynamics (MD) simulation is to simulate the time evolution of a system. The classical MD simulation methods are in principle based on atomistic level processes. In classical MD simulation, a molecular system is treated as a collection of classical point particles and its dynamic evolution is governed by Newtonian mechanics. In order to determine the forces acting on each particle in a particular system, an interatomic potential function is used. The point like particles interact according to a given potential energy $U(\mathbf{r}_1, \mathbf{r}_2, \mathbf{r}_3, ..., \mathbf{r}_N)$, where N is the number of particles in the system. The evolution of the system is computed in simulation time steps of a small time period δt. In classical MD simulations, the es-

sential quantity to be known is the potential energy, since a system of classical point particles obeys Newton's equation of motion

$$\mathbf{f}_i = m_i \frac{d^2\mathbf{r}_i}{dt^2} = -\nabla_i U(\mathbf{r}_1, \mathbf{r}_2, \mathbf{r}_3, ..., \mathbf{r}_N) \tag{1.1}$$

where the index i refers to one of the particles in the system and m_i is the mass of atom i.

For studying simple atomistic systems, the use of classical MD methods is well justified. The simple model potentials take into account only two particle interactions. For simple systems, these model potentials may provide an adequate description of the system. However, the use of classical MD to study more complex systems, such as carbon and silicon structures, would require a more tedious work to construct many-body empirical classical model potentials. Since the electrons are not sharply localized in the neighborhood of their parent ions in such complex systems, electronic effects must be taken into account in these model potentials. But the classical approaches using empirical many body potentials, proposed for calculating the properties of silicon and carbon, still do not guarantee the correct description of such complex systems. Therefore, MD simulations of more complex molecular systems employed to calculate their macroscopic properties with sufficient accuracy require quantum mechanical treatments. The quantum mechanical MD simulation methods are more feasible than classical MD methods to simulate the exact motion of atoms within a system and extract macroscopic properties from the microscopic description of the system connected with electronic influence.

First principles, or *ab initio*, MD methods provide an accurate description of quantum mechanical behavior of molecular systems. However, MD simulations using first principles approach would be much more time consuming and computationally heavy. The most widely known first principles approach to MD is Car Parrinello (CP) method. Car and Parrinello extended MD to include electronic effects within the density functional framework [29]. In computer simulation studies of molecular systems, there is a clear need to extend system sizes and simulation time scales. The system size must be large enough to yield reliable macroscopic properties. In addition,

the simulation time scales for the study of molecular systems must be long enough to observe the physical effects. The first principles methods are highly accurate but the system size that can be handled is restricted to tens, at most a couple of hundred atoms. In addition, high computational workload due to the explicitly included electronic effects limits the duration of the simulation.

In principle, of course, the Hamiltonian of the system depends on all electron-electron and electron-nuclear interactions. However, to obtain a more tractable problem, we make the tight binding (TB) approximation. As a semi-empirical method, TB approximation is a simplified but still quantum mechanical approach to molecular dynamics. In other words, TBMD methods are in between *ab initio* or first principles simulation methods and classical models for molecular dynamics, either as far as the overall numerical efficiency and/or as far as the accuracy were concerned [18]. The TB model assumes that each electron is well localized around a given nucleus. If this is the case, then the atomic description is not completely irrelevant but the overlap of the atomic wave functions require corrections to the picture of isolated atoms.

The TBMD program employed in this thesis has two main stages [25]. We start with an initial tube structure and consider the evolution of the system. In our calculations, electronic effects are treated in a natural way using a tight binding approximation method. In the first stage of our calculations, the electronic structure of tubes are calculated by a TB Hamiltonian. In addition, the contribution to the atomic forces due to the electronic structure is calculated in the first stage. Then the contribution due to an empirical repulsive potential is added trivially. In other words, nuclear motions are caused by the total force that is calculated from two main contributions. Then in the second stage we use the total force on each of the nuclei in the classical equations of motion to advance the nuclei. We will discuss TBMD simulation techniques employed in this thesis in more detail in Chapter 3.

1.2 Hybridization in Carbon and Silicon Atoms

Each carbon atom has six electrons which occupy $1s^2$, $2s^2$, and $2p^2$ atomic orbitals. The $1s^2$ orbital contains two strongly localized electrons, and they are called core electrons. Four electrons occupy the $2s^2 2p^2$ orbitals, and these more weakly localized electrons are called valance electrons. In the crystalline phase the valance electrons give rise to $2s$, $2p_x$, $2p_y$, and $2p_z$ orbitals. Since the energy difference between $2s$ and $2p$ levels in carbon is small compared with the binding energy of the chemical bonds, the electronic wave functions for these four valance electrons can readily mix with each other. This mixing of atomic orbitals is called hybridization, and specifically the mixing of the wave function of an electron which is in $2s$ state with the wave functions of the electrons in $n = 1, 2, 3$ $2p$ orbitals is called sp^n hybridization [1]. The strong localization of the electrons in the inner atomic $1s$ orbitals results in hybridizations involving only valance electrons in $2s$ and $2p$ orbitals. There is a very small overlap between $1s$ orbitals on adjacent atomic sites in the solid. In other words, $1s$ core orbitals do not generally affect the solid properties of carbon based materials.

Three possible hybridizations occur in carbon: sp, sp^2 and sp^3. The mixing of wave functions of electrons occupying different atomic orbitals is essential for determining the dimensionality and structures of carbon based materials. In other words, possible structures of carbon materials are closely related to the sp^n hybridization. Carbon in the only element that can form structures from zero dimensions to three dimensions. In sp^n hybridization, $(n+1)$ σ bonds per carbon atom are formed, these σ bonds making a skeleton for the n dimensional structure [1]. For example, in sp^3 hybridization, four σ defining a regular tetrahedron are sufficient to form a three dimensional structure, which is known as the diamond structure. In addition, sp^2 hybridization forms a planar structure in two dimensional graphite known as graphene sheet [1]. It is interesting that sp^2 hybridization also forms a local planar structure in the forms of cylinders, which is called carbon nanotubes.

Although three possible hybridizations occur in carbon, the other group IV element silicon exhibits primarily sp^3 hybridization. In other words, sp^3 hybridization

is more stable in silicon. Because sp^2 hybridization is stable in carbon, it can easily form two dimensional planar structures and nanotubes composed of only sp^2 bonds. However, silicon is well known as just being in the form of diamond. Due to the lack of sp^2 hybridization in silicon, we might conclude that silicon cannot form local planar structures and nanotubes. The crystalline structure of three dimensional silicon is cubic diamond similar to that of carbon diamond. However, unlike the carbon counterpart, a graphene-like structure and single walled hexagonal silicon nanotube has not been found in the nature yet. It is largely because silicon prefers sp^3 hybridization rather than sp^2 hybridization. But nevertheless many researchers do not rule out the possibility of the existence of silicon nanotubes. Recently many authors investigated silicon nanotubes [22-34].

1.3 Carbon and Silicon Nanotubes

A single wall carbon nanotube (SWCNT) is basically described as a graphene sheet (a single layer of graphite) rolled into a cylindrical shape so that the structure is one dimensional with axial symmetry. The diameter of a carbon nanotube is of nanometer size and the length of of the tube can be up to several micrometers. Because of its very small size and the special electronic properties, a SWCNT is a unique material. Because of the large variety of possible geometrical structures, which are determined by the chiral vector, SWCNTs provide a family of structures with different diameter and chiralities [1]. SWCNTs also have unique mechanical properties. For a detailed discussion of the unusual properties of SWCNTs we refer to the book by Dresselhaus *et al* [1].

Aforementioned it is known that graphite is a stable structure for carbon, whereas for silicon diamond structure is the most stable [1]. In other words, the sp^2 hybridization is more stable in carbon, whereas the sp^3 hybridization is more stable in silicon. However, despite the difficulties having an sp^2-like (graphenelike) structure for silicon, many researchers do not completely rule out the possibility of the existence of single wall SW silicon h-NTs, i.e. silicon nanotubes with the structures of carbon

nanotubes. In the literature, two types of silicon nanotubes are studied using *ab initio* calculations: SW silicon hexagonal nanotubes (h-NTs) [22,24,25,27-33] and SW silicon gear-like nanotubes (g-NTs) [25-27]. Like SWCNTs, the analogous SW silicon hexagonal nanotubes (h-NTs) are formed by rolling-up the graphene-like silicon sheets. In addition, gear-like nanotubes (g-NTs) are formed by rolling the (111) sheet of the diamond structure.

In this thesis, silicon h-NTs are built in analogy with SWCNTs. SW silicon h-NT structures are simply constructed by folding a graphenelike sheet of silicon into a cylindrical shape. The periodic boundary conditions are applied along the axial direction of the tube. Like hypothetical silicon h-NTs, SWCNTs are formed by rolling up infinite planar hexagonal lattice into a cylinder. Since SW silicon h-NTs have similar geometric structures with SWCNTs, we introduce the structure of graphene structure (analogous to graphenelike silicon structure) and SWCNT structure (analogous to SW silicon h-NT). In general, we will call both SWCNT and SW silicon h-NT as SW hexagonal nanotube, since they are formed by rolling up planar hexagonal

1.3.1 The Geometry of a SW Hexagonal Nanotube

Each single wall hexagonal nanotube could be regarded as a rolled-up graphite (or graphite-like for silicon) sheet in the cylindrical form. Generally, single wall nanotubes can be characterized by two integers (n, m). Starting from a graphite sheet with the primitive lattice vectors $\mathbf{a}_1$, $\mathbf{a}_2$ making an angle of 60^o, the (n, m) tube is a cylinder with the axis running perpendicular to the chiral vector $\mathbf{C}_h$, so that atoms separated by $n\mathbf{a}_1 + m\mathbf{a}_2$ are wrapped onto each other. (See Fig. 1.1) The chiral vector

$$\mathbf{C}_h = n\mathbf{a}_1 + m\mathbf{a}_2 \tag{1.2}$$

where n and m are integers. The integer pair (n, m) completely describe the geometry of a nanotube. Because of the rotational symmetry of the $2D$ hexagonal lattice, it is only necessary to consider n and m such that $0 \leq |m| \leq n$. The cylindrical shape of the tube exhibits a spiral conformation or chirality. This fact provides many possible

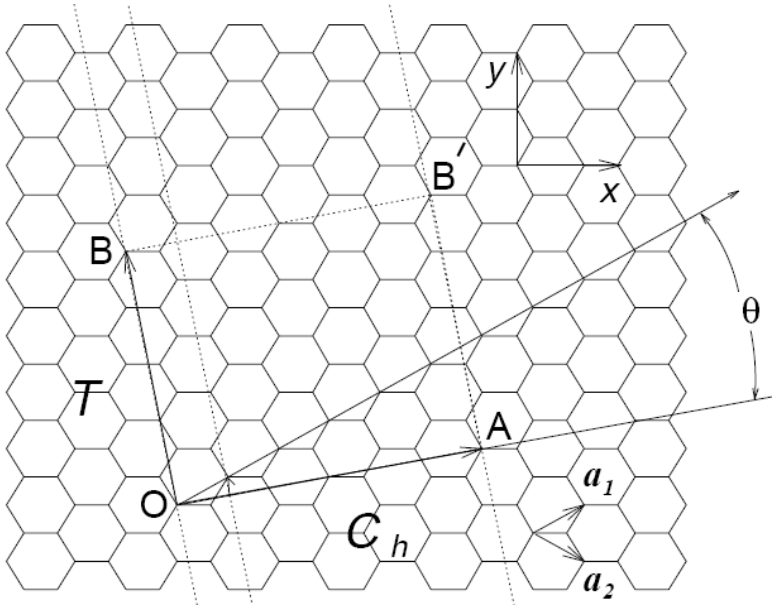

Figure 1.1: The unrolled hexagonal lattice of a nanotube (from Ref. 1).

structures for nanotubes, although the basic shape of the nanotube wall is a cylinder. An armchair nanotube corresponds to the case of $n = m$, and a zigzag nanotube corresponds to the case of $m = 0$. All other chiral (n,m) pairs correspond to chiral nanotubes. Chiral nanotubes exhibit a spiral symmetry whose mirror image cannot be superposed on the original one, whereas the mirror image of an armchair or zigzag nanotube has an identical structure to the identical one. (See Fig. 1.2) In the figure the terminations of the nanotubes are shown. However in this thesis we focus on the periodic structure along the nanotube axis and in our studies we apply periodic boundary conditions along the axial direction.

Referring to Fig. 1.1, in the x, y coordinates the real space unit vectors $\mathbf{a}_1$ and $\mathbf{a}_2$ of the hexagonal lattice can be written as:

$$\mathbf{a}_1 = a_0\sqrt{3}(\frac{\sqrt{3}}{2}, \frac{1}{2})\mathbf{a}_2 = a_0\sqrt{3}(\frac{\sqrt{3}}{2}, -\frac{1}{2}) \tag{1.3}$$

with a_0 denoting the nearest neighbor distance in the hexagonal lattice, which is equal to $1.42\mathring{A}$ in the graphene. The lattice constant of the hexagonal lattice is defined as $a = a_0\sqrt{3}$ and is simply equal to $a = 1.42\sqrt{3} = 2.46\mathring{A}$ in the graphene. The inner

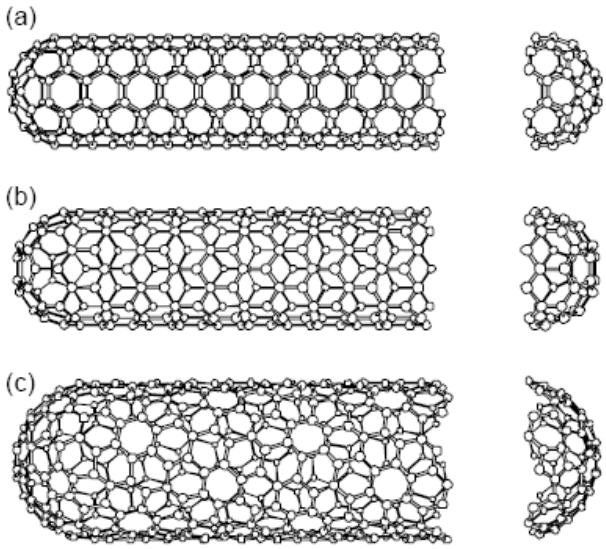

Figure 1.2: Classification of nanotubes: (a) armchair, (b) zigzag, and (c) chiral nanotubes (from Ref. 1).

products between the primitive lattice vectors $\mathbf{a}_1$ and $\mathbf{a}_2$ are

$$\mathbf{a}_1.\mathbf{a}_1 = \mathbf{a}_2.\mathbf{a}_2 = a^2, \mathbf{a}_1.\mathbf{a}_2 = \frac{a^2}{2} \tag{1.4}$$

where a is the lattice constant. Then the circumferential length L of the cylinder formed by rolling the hexagonal planar structure is given by

$$L = |\mathbf{C}_h| = \sqrt{\mathbf{C}_h.\mathbf{C}_h} = a\sqrt{n^2 + m^2 + nm} \tag{1.5}$$

and the radius of the cylinder is

$$r = \frac{L}{2\pi} = \frac{a}{2\pi}\sqrt{n^2 + m^2 + nm} \tag{1.6}$$

Briefly, the structure of a SWNT, which is formed by rolling a graphite (or graphite-like for silicon) sheet in the cylindrical form, is simply specified by the chiral vector. In Fig. 1.1 the vector $\overrightarrow{OA}$ define the chiral vector $\mathbf{C}_h$ and the vector $\overrightarrow{OB}$ define the translational vector $\mathbf{T}$ of the nanotube. The vector $\mathbf{T}$ is parallel to the nanotube axis and is normal to the chiral vector $\mathbf{C}_h$ in the unrolled hexagonal lattice structure. The translational vector $\mathbf{T}$ and some other vectors, which are derived from

the chiral vector, should be defined in order to completely specify the structure of the nanotube.

For a detailed discussion of the characteristic vectors and other related parameters of nanotubes we refer to the book by Dresselhaus *et al* [1]. The book also offers a program for generating parameters and atomic coordinates of a general (n, m) nanotube.

Chapter 2

PRELIMINARIES

This chapter offers first an overview on materials simulation methods at the atomic scale. The methods of modeling the atomic interactions can roughly be divided into three categories. The first principles, or *ab initio*, methods are the most rigorous ones. Only a few well controlled approximations to exact quantum mechanics are made. Semi-empirical methods contain more drastic approximations and may also contain empirically defined parameters. Empirical methods are a group of methods that are tuned to reproduce an empirically defined fitting set. The three categories, their drawbacks and benefits are briefly described in Section 2.1. In this thesis the emphasis is on semi-empirical tight-binding molecular dynamics (TBMD). Therefore it is discussed in detail followed by an introduction to the molecular dynamics (MD) and tight binding (TB) formalism. In section 2.2 we discuss the basics of MD scheme while in section 2.3 we present the basic theory of TB formalism. The TB model coupled with MD will be introduced in Chapter 3.

2.1 Simulation Methods

Modeling of matter at the microscopic level is based on a comprehensive description of the constituent particles. In fact, such a description must in principle be based on quantum mechanics. For a general atomic or molecular system consisting of electrons and nuclei, the interactions and evolution of such a system is governed by the time dependent Schrödinger equation. The most rigorous quantum mechanical approach to the systems of interest are called first principles methods. They do not employ any empirical parameters in the calculation. Exact quantum mechanical calculations of the properties of the systems at the nano scale are based on solving the many body

time dependent Schrödinger equation and obtaining the many body wave function $\Psi(r_1, ..., r_n, t)$. These methods explicitly include electronic effects and provide highly accurate electronic structures. Unfortunately these calculations are computationally heavy, therefore limits the system size and simulation time. First principles approach to molecular dynamics have been used, for example, for structural studies of small carbon and silicon clusters. Because of the absence of empirical fitting, the results of first principles calculations are very reliable and serve as a useful reference for testing the accuracies of more approximate approaches.

Classical molecular dynamics (MD), on the other hand, represents atoms or molecules as point particles interacting through forces that depend on the separation of these objects. Classical MD simulations determine the force laws between particles from empirical potentials that have been fitted to reproduce some properties of the system that are determined either from experimental data or from first principles calculations. In other words, the classical approximation to the quantum mechanical nature of a system is the result of adapting the potential arising from the interactions between particles to a variety of different kinds of information. These include the results of quantum mechanical first principles energy and electronic structure calculations and experimental data obtained by thermodynamic and spectroscopic means. Although model potentials are not ideal for the study of the properties of molecular systems, they are used because they are simple to implement. Furthermore, the classical approach using model potentials allow the simulation of systems consisting of up to millions of atoms.

The simplest approximation for the model potentials takes into account only two-particle interactions. For simple systems, such as a collection of noble gas atoms, these models may provide an adequate description of the system. In the atomic state, noble gases have completely filled electronic shells which is a highly stable configuration. From the point of view of the band structure, the noble gases are fine examples of extreme tight binding solids. Since all the electrons can be considered to be core electrons, there is a very little electronic density between ion cores and

all the electrons remain well localized in the neighborhood of their parent ion cores. Therefore, such simple systems can be treated as a collection of classical particles and the results obtained by using the classical molecular dynamics approach for studying such simple systems are adequately accurate.

However, using classical MD to study more complex systems, such as carbon and silicon structures, would require a more tedious work to construct many-body empirical classical potentials. Moreover, the classical approaches using empirical potentials, proposed for calculating the properties of silicon and carbon, do not guarantee the correct description of such complex systems in various environments and in different phases. Stillinger-Weber (SW) potential, a many-body potential for silicon, is the most widely used model potential for calculating the properties of liquid silicon [16], [17]; however, the accuracy of the results is still far from being satisfactory. The electrons in carbon and silicon structures, are not sharply localized in the neighborhood of their parent ion cores. Therefore, electronic effects must be taken into account.

But most of these empirical potential methods are classical in nature and cannot account for electronic effects in carbon and silicon systems. In the first principles methods case, on the other hand, quantum mechanical interactions among electrons and ion cores receive rigorous treatment based on solving the many body time dependent Schrödinger equation. Unfortunately to perform such calculations on reasonable size samples would require heavy computational resources. This ensures that the exact quantum mechanics calculations cannot be considered as an efficient way to study such complex systems, as for the case of classical dynamics approaches.

In this thesis, we employed a semi-empirical Tight-Binding Molecular Dynamics (TBMD) simulation technique for single walled (SW) hexagonal silicon nanotubes (h-NTs). We start with an initial tube structure and consider the evolution of the system into two stages. The electronic structure of the carbon and silicon nanotubes are calculated by a TB Hamiltonian. Following an elaborate electronic structure calculation, we determine the quantum mechanical forces, so called Hellmann-Feynman forces, on each of the nuclei. In other words, once the full spectrum of eigenvalues and eigenvec-

tors of the TB Hamiltonian is determined, we can calculate Hellmann-Feynman forces straightforwardly. Hellmann-Feynman Theory and Hellmann-Feynman contribution to the atomic forces are discussed in Chapter 3. Furthermore, the other contribution to the total force on nuclei is the result of the effective repulsive potential, which is expressed as a 4th-order polynomial with the argument of the sum of pairwise potentials between atoms. In fact, as discussed in Chapter 3, the effective repulsive potential and pairwise potential are known analytically.

Finally, in the second stage, the total force on each of the nuclei is used in the classical equations of motion to advance the nuclei. In other words, the dynamic motions of nuclei are still governed by Newtonian mechanics and described by the classical molecular dynamics. The nuclei positions, velocities and accelerations are updated according to the velocity Verlet algorithm, as discussed in Chapter 2. This procedure is repeated for each molecular dynamics time step.

2.2 Basics of Molecular Dynamics

In this section, the general approach used in classical MD simulations and the techniques used to solve the classical equations of motion are discussed. In MD, to account for the movement of the particles in the system over time, the simulation is broken into a series of sequential time steps. Given an initial set of positions, velocities and accelerations, the subsequent time evolution of the system is determined. In order to find out, how the system evolves in time, equations of motion for each particle are solved on step by step basis. This is called the *integration of the equation of motion*. The equations of motion for each particle are numerically integrated forward in simulation time steps using finite difference methods. Most of the MD simulation codes tend to use the Verlet type algorithms or the predictor-corrector algorithm as a finite difference method to solve the differential equations of motion numerically.

2.2.1 Integration of Equations of Motion

Given the particle positions, velocities, accelerations and other dynamic information at time t, we attempt to obtain the positions, velocities etc. at a later time $t + \delta t$, to a sufficient degree of accuracy. In addition, to start a simulation, the set of positions, velocities and accelerations should be assigned initially to the particles. The macroscopic properties of the system of interest are then calculated at each MD simulation time step.

A velocity Verlet algorithm has been chosen for the program that is used in this thesis. In comparison to other integration algorithms, such as Gear's predictor-corrector algorithm, it is relatively simple. There are several integration schemes of various complexity and order [31]. But the discussion is limited to the the velocity Verlet algorithm, which is employed in this thesis, and the predictor-corrector algorithm. The predictor-corrector integration scheme is considered computationally heavy, however, it has an accuracy advantage and therefore it is used most widely in MD simulations [31].

Gears predictor-corrector method is composed of three steps: prediction, evaluation, and correction. In the prediction step, an estimate of particle positions, velocities etc. at a later time $t + \delta t$ is obtained by Taylor expansion about time t:

$$\begin{aligned}
\mathbf{r}^p(t+\delta t) &= \mathbf{r}(t) + \delta t\mathbf{v}(t) + \frac{1}{2}\delta t^2\mathbf{a}(t) + \frac{1}{6}\delta t^3\mathbf{b}(t) + ... \\
\mathbf{v}^p(t+\delta t) &= \mathbf{v}(t) + \delta t\mathbf{a}(t) + \frac{1}{2}\delta t^2\mathbf{b}(t) + ... \\
\mathbf{a}^p(t+\delta t) &= \mathbf{a}(t) + \delta t\mathbf{b}(t) + ... \\
\mathbf{b}^p(t+\delta t) &= \mathbf{b}(t) + ...
\end{aligned} \tag{2.1}$$

where the superscript p indicates that the values are the predicted values. Since Taylor series is an infinite series, the predicted values will have slight errors due to the truncation of the series after the third order term. However, left uncorrected over many time steps, these slight truncation errors can build up to significant values, resulting in inaccurate data. Therefore, it is necessary to correct the values predicted in Eq. (2.1). In the evaluation step, from the new positions $\mathbf{r}^p(t + \delta t)$, the forces at

time $t + \delta t$, and hence the correct accelerations $\mathbf{a}^c(t + \delta t)$ are calculated. Comparing corrected accelerations for each particle with the predicted acceleration from Eq. (2.1), the size of the error in the prediction step is estimated:

$$\Delta\mathbf{a}(t + \delta t) = \mathbf{a}^c(t + \delta t) - \mathbf{a}^p(t + \delta t) \tag{2.2}$$

Finally, in the correction step, the corrected positions, velocities, etc can be written. Typically

$$\begin{aligned}
\mathbf{r}^c(t + \delta t) &= \mathbf{r}^p(t + \delta t) + c_0\Delta\mathbf{a}(t + \delta t) \\
\mathbf{v}^c(t + \delta t) &= \mathbf{v}^p(t + \delta t) + c_1\Delta\mathbf{a}(t + \delta t) \\
\mathbf{a}^c(t + \delta t) &= \mathbf{a}^p(t + \delta t) + c_2\Delta\mathbf{a}(t + \delta t) \\
\mathbf{b}^c(t + \delta t) &= \mathbf{b}^p(t + \delta t) + c_3\Delta\mathbf{a}(t + \delta t))
\end{aligned} \tag{2.3}$$

A detailed discussion of how to choose the coefficients c_0, c_1, c_2, c_3, ... can be found in Ref [31]. A typical stepwise MD simulation, based on the Gears predictor-corrector algorithm, works as follows:

(a) set the initial positions, velocities, accelerations etc. at time t;

(b) 'predict' the positions, velocities, accelerations etc. at time $t + \delta t$ using the current values of these quantities;

(c) 'evaluate' the forces, and hence the correct accelerations at time $t + \delta t$, from new positions $\mathbf{r}^p(t + \delta t)$;

(d) 'correct' the predicted values of positions, velocities, accelerations etc. using new accelerations;

(e) store new positions, velocities, accelerations etc

(f) calculate the physical quantities of interest.

The steps from (b) to (f) represent one molecular dynamics step. The molecular dynamics step is repeated as long as the simulation is run, so a discrete time development of the system and its dynamics is obtained.

The MD simulation program employed in this thesis updates atomic positions, velocities and accelerations according to the velocity Verlet algorithm. The integration

equations of the velocity Verlet algorithm are

$$\begin{aligned} \mathbf{r}(t+\delta t) &= \mathbf{r}(t) + \delta t \mathbf{v}(t) + \frac{1}{2}\delta t^2 \mathbf{a}(t) \\ \mathbf{v}(t+\delta t) &= \mathbf{v}(t) + \frac{1}{2}[\mathbf{a}(t) + \mathbf{a}(t+\delta t)] \end{aligned} \tag{2.4}$$

The workings of a molecular dynamics simulation using the velocity Verlet integration algorithm can be represented as follows:

(a) set the initial positions, velocities, accelerations etc. at time t;

(b) update the positions;

(c) calculate the forces, and hence the accelerations at time $t + \delta t$, from new positions $\mathbf{r}^p(t + \delta t)$;

(d) update the velocities;

(e) store new positions, velocities, accelerations;

(f) calculate the physical quantities of interest.

From the beginning of the simulation, the steps from (b) to (f) are repeated as long as the simulation is run.

2.2.2 The Verlet Neighbor List

The most time consuming part of a molecular dynamics simulation is the evaluation of the forces on each particle from the particle positions at each simulation time step. Calculation of the forces on each particle require the determination of the potential. Most of the model potentials are expressed analytically as a function of the relative distances between constituent particles. Therefore, once the distances between particles are calculated, the potential due to particle interaction are evaluated. Then the forces on each particle, hence accelerations are calculated straightforwardly. In order to reduce implementation time, in most cases, only the interactions of a particle with the particles within a potential cutoff sphere are taken into account. If particles are separated by distances greater than the potential cutoff, the program skips to the end of the force calculation loop and considers the next neighbor.

In our calculations, short range interactions are assumed and only the nearest neighbor interactions are taken into account. In other words, we choose the cutoff distance between the nearest neighbor and the next nearest neighbor of carbon or silicon atoms in the system of interest. Testing whether atoms are separated by less than the cutoff distance is a part of the overall computation. At the first step in a MD simulation, a list is constructed of all neighbors of each atom, and from time to time the neighbor list is reconstructed.

For the beginning of the molecular dynamics simulation, the simulation time step value must be set. The time step δt must be significantly smaller than the typical time taken for a particle to travel its own length. Since the new positions, velocities etc for each particle at time $t + \delta t$ are computed as an approximation to the values of these quantities at time t, the smaller the simulation time step, the more accurately will the solution follow the correct trajectory. On the other hand, a time step that is too small wastes computational resources. Time step length is therefore a compromise between accuracy and stability. Thus the extent to which δt can be increased without prejudicing the stability of the simulation should be investigated. The typical time step is approximately 1 fs in equilibrium simulations.

2.3 Separation of Electronic and Nuclear Motions

For a general system with N nuclei and n electrons, the Hamiltonian can be written as

$$H(R, r) = T_N(R) + H_{el}(r) + V(R, r), \tag{2.5}$$

where R and r are the collective indexes used to denote, respectively, the coordinates of the nuclei and electrons. The first and second terms of the Hamiltonian correspond to the kinetic energy of the nuclei and the energy of the electron system, respectively. The last term $V(R, r)$ includes all the interaction energies among nuclei themselves and between nuclei and electrons. Moreover, the electronic Hamiltonian $H_{el}(r)$ can

be written as

$$H_{el}(r) = T_e + V_{ee}, \tag{2.6}$$

where T_e represents kinetic energy of the electrons and V_{ee} includes all electron-electron interaction energies. Various terms of the Hamiltonian in Eq. (2.3.1) are explicitly given by

$$T_e = \sum_i^n (-\frac{\hbar^2}{2m_e})\nabla_i^2, \tag{2.7}$$

$$V_{ee} = \frac{1}{2}\sum_{i\neq j}^{n} \frac{1}{r_{ij}}, \tag{2.8}$$

$$H_N(R) = \sum_k^N (-\frac{\hbar^2}{2M_k})\nabla_k^2, \tag{2.9}$$

and

$$V(R,r) = \frac{1}{2}\sum_{k\neq l}^{N} \frac{Z_k Z_l}{R_{kl}} - \sum_k^N \sum_i^n \frac{Z_k}{|R_k - r_i|} \tag{2.10}$$

where R_k, M_k, and Z_k represents the position, mass, and charge of the k^{th} nucleus respectively, and m_e is the electron mass.

2.3.1 Adiabatic Representation

Based on the rationale that the nuclear mass is much larger than the electron mass, we can use an *adiabatic approximation* in order to describe the dynamics of the general system described by the Hamiltonian (2.5). The nuclei with heavy mass move much slower than the electrons with light mass, and therefore nuclear kinetic energies are generally much smaller than those of electrons. If we fix the position of the nuclei (R fixed), then the eigenfunctions of electrons corresponding to the fixed configuration of the nuclei would be determined by the following Hamiltonian equation,

$$[H_{el}(r) + V(R,r)]\phi_n(R,r) = \epsilon_n(R)\phi_n(R,r) \tag{2.11}$$

where $\phi_n(R,r)$ and $\epsilon_n(R)$ are called the *adiabatic* electronic wave functions and energy eigenvalues of the electrons with fixed nuclear coordinates R. Since the adiabatic eigenfunctions $\phi_n(R,r)$ form a complete orthonormal set, the molecular wave function $\Psi(R,r)$ can be can be expanded in the adiabatic basis set $\phi_n(R,r)$, i.e.

$$\Psi(R,r) = \sum_n \chi_n(R)\phi_n(R,r) \tag{2.12}$$

where $\chi_n(R)$ is the corresponding nuclear wave function in the adiabatic representation. The molecular Schrödinger equation is

$$H_n(R,r)\Psi(R,r) = E\Psi(R,r). \tag{2.13}$$

By substituting the expansion in Eq. (2.12) into Eq. (2.13) and integrating over the electron coordinates, we obtain the coupled equations

$$[T_N(R) + \epsilon_m(R)]\chi_m(R) + \sum_n \wedge_{mn}(R)\chi_n(R) = E\chi_m(R) \tag{2.14}$$

where $\wedge_{mn}(R)$ is the non-adiabatic coupling operator which arises from the action of the nuclear kinetic energy operator $T_N(R)$ on the electron wave function. Explicitly

$$\wedge_{mn}(R) = -\hbar^2 \sum_i \frac{1}{M_i}[A^i_{mn}\frac{\partial}{\partial R_i} + \frac{1}{2}B^i_{mn}] \tag{2.15}$$

where A^i_{mn} and B^i_{mn} are defined as

$$A^i_{mn} = \langle\phi_m|\frac{\partial}{\partial R_i}|\phi_n\rangle = \int \phi^*_m \frac{\partial}{\partial R_i}\phi_n dr \tag{2.16}$$

$$B^i_{mn} = \langle\phi_m|\frac{\partial^2}{\partial R_i^2}|\phi_n\rangle = \int \phi^*_m \frac{\partial^2}{\partial R_i^2}\phi_n dr \tag{2.17}$$

It is clear that the operator $\wedge_{mn}(R)$ is the result of the non-adiabatic coupling between different adiabatic states.

The rigorous approach to get the nuclear wave function $\chi_n(R)$ in the adiabatic representation is to solve the coupled Schrödinger equation (2.14). However, since the adiabatic approximation assumes that the nuclear kinetic energies are much smaller

than those of electrons, the non-adiabatic terms A_{mn} and B_{mn}, which result from the nuclear motions, are generally small. In other words, the dependence of A_{mn} and B_{mn} on nuclear coordinates R is relatively weak compared to that of $\epsilon_n(R)$. Consequently, neglecting the non-adiabatic coupling in Eq. (2.14), we obtain the adiabatic approximation for the nuclear wave function

$$[T_N(R) + \epsilon_n(R)]\chi_n(R) = E\chi_n(R) \tag{2.18}$$

It is clear, in the adiabatic approximation, that the energy eigenvalues defined in Eq. (2.11) is the adiabatic potential for the nuclear motion. Replacing the adiabatic potential $\epsilon_n(R)$ by the notation $V_n(R)$, one obtains the Born-Oppenheimer approximation

$$[T_N(R) + V_n(R)]\chi_n(R) = E\chi_n(R) \tag{2.19}$$

Therefore, as a consequence of the adiabatic approximation, we achieve a complete separation of electronic motion from that of nuclei. Then we find electronic eigenvalues at given fixed nuclear coordinates R and we use $\epsilon_n(R)$ as the potential for the nuclei. Finally using the Born-Oppenheimer approximation Eq. (2.19), one can solve the nuclear dynamics problem. In the next subsection, we will show that how we can simply calculate the forces on the nuclei from the adiabatic potential without the need of the adiabatic electronic wave functions $\phi_n(R, r)$. As we calculate the forces on each nuclei, the rest will be a classical molecular dynamics problem.

2.3.2 Hellmann-Feynman Theory

The Hellmann-Feynman theory provides a convenient means to compute forces on the nuclei for a molecular system in the adiabatic or Born-Oppenheimer approximation. It is named for its independent provers Hans Hellmann (1936) and Richard Feynman (1939). Consider a system where the motions of electrons are governed by the Hamiltonian $H(\lambda)$ that depends on some parameters λ. Let $|\phi(\lambda)\rangle$ be an eigenstate of $H(\lambda)$ with an energy eigenvalue $\epsilon(\lambda)$.

$$H(\lambda)|\phi(\lambda)\rangle = \epsilon(\lambda)|\phi(\lambda)\rangle \tag{2.20}$$

Since the adiabatic eigenstates $|\phi(\lambda)\rangle$ form a complete orthonormal set, the adiabatic energy eigenvalue $\epsilon(\lambda)$ can be expressed as the expectation value of the Hamiltonian $H(\lambda)$

$$\epsilon(\lambda) = \langle\phi(\lambda)|H(\lambda)|\phi(\lambda)\rangle \tag{2.21}$$

Differentiating both sides with respect to the parameter λ yields

$$\frac{\partial\epsilon(\lambda)}{\partial\lambda} = \langle\frac{\partial\phi(\lambda)}{\partial\lambda}|H(\lambda)|\phi(\lambda)\rangle + \langle\phi(\lambda)|H(\lambda)|\frac{\partial\phi(\lambda)}{\partial\lambda}\rangle + \langle\phi(\lambda)|\frac{\partial H(\lambda)}{\partial\lambda}|\phi(\lambda)\rangle \tag{2.22}$$

Using the fact that $|\phi(\lambda)\rangle$ is an eigenstate of the Hamiltonian $H(\lambda)$ with energy eigenvalue $\epsilon(\lambda)$, above equation can be simplified as

$$\begin{aligned}
\frac{\partial\epsilon(\lambda)}{\partial\lambda} &= \epsilon(\lambda)\langle\frac{\partial\phi(\lambda)}{\partial\lambda}|\phi(\lambda)\rangle + \epsilon(\lambda)\langle\phi(\lambda)|\frac{\partial\phi(\lambda)}{\partial\lambda}\rangle + \langle\phi(\lambda)|\frac{\partial H(\lambda)}{\partial\lambda}|\phi(\lambda)\rangle \\
&= \epsilon(\lambda)[\langle\frac{\partial\phi(\lambda)}{\partial\lambda}|\phi(\lambda)\rangle + \langle\phi(\lambda)|\frac{\partial\phi(\lambda)}{\partial\lambda}\rangle] + \langle\phi(\lambda)|\frac{\partial H(\lambda)}{\partial\lambda}|\phi(\lambda)\rangle \\
&= \epsilon(\lambda)\frac{\partial}{\partial\lambda}\langle\phi(\lambda)|\phi(\lambda)\rangle + \langle\phi(\lambda)|\frac{\partial H(\lambda)}{\partial\lambda}|\phi(\lambda)\rangle
\end{aligned} \tag{2.23}$$

However, since $|\phi(\lambda)\rangle$ is normalized, the first term vanishes and we obtain

$$\frac{\partial\epsilon(\lambda)}{\partial\lambda} = \langle\phi(\lambda)|\frac{\partial H(\lambda)}{\partial\lambda}|\phi(\lambda)\rangle \tag{2.24}$$

which is known as the Hellmann-Feynman theory.

Since the adiabatic or Born-Oppenheimer approximation assumes fixed nuclear geometries, we can take nuclear coordinates R as parameters. In addition, adiabatic eigenvalues $\epsilon(R)$ of the electrons at the given fixed nuclear coordinates, defined in Eq. (2.11), is the adiabatic potential for the nuclear motion. (See Eq. (2.18) and Eq. (2.19)) Consequently, the Hellmann-Feynman theory provides that

$$\frac{\partial\epsilon(R)}{\partial R} = \langle\phi(R)|\frac{\partial H(R)}{\partial R}|\phi(R)\rangle \tag{2.25}$$

where $H(R)$ is the Hamiltonian for electronic motion, which is defined as

$$H(R,r) = H_{el}(r) + V(R,r) \tag{2.26}$$

where H_{el} is the electronic Hamiltonian and $V(R,r)$ includes all the electron-nuclear and nuclear-nuclear interactions. Thus the force acting on the ith nucleus can now be straightforwardly calculated from the adiabatic potential $\epsilon(R)$ via the Hellmann-Feynman theory

$$\overrightarrow{f}_i = -\nabla_i \epsilon(R) \tag{2.27}$$

Eq. (2.27) states that the force acting on the ith nucleus is simply the negative gradient of the adiabatic eigenvalue or potential $\epsilon(R)$ with respect to the ith nuclear coordinate. This is a great simplification because at each molecular time step the forces needed to move atoms can be calculated numerically without the need of electronic wave functions $\phi_n(R,r)$. For simplicity, we will call $\overrightarrow{f}_i$ the Hellmann-Feynman contribution to the atomic forces. Up to now, we left out the nuclear-nuclear interactions in our derivation. In fact, as discussed in Chapter 3, the repulsive potential due to nuclear-nuclear interactions are short ranged and known analytically. The forces due to the repulsive potential term can be trivially calculated and added to the right side of Eq. (2.27). Finally, the effective repulsive potential and the numerical Hellmann-Feynman contribution to the total force will be discussed in more detail in the third chapter.

2.4 The Tight Binding Formalism

The full periodic crystal Hamiltonian, H, in the vicinity of each lattice point, is approximated by the Hamiltonian of a single atom located at the lattice point. Here we also assume that, for an atom at the origin, the bound levels of the atomic Hamiltonian, H_{at}, are well localized. We can write the atomic Schrödinger equation as

$$H_{at}\psi_n = E_n\psi_n, \tag{2.28}$$

where ψ_n is a bound level of the atomic Hamiltonian, H_{at}, and E_n is the energy of the corresponding atomic level. Since we assume that the bound levels of the atomic Hamiltonian are well localized, we require that $\psi_n(\mathbf{r})$ be very small at a distance greater than the lattice constant. In the extreme case in which the electronic density between ion cores is very little, as for the noble gases, the crystal Hamiltonian, H, differs from the Hamiltonian of a single isolated atom, H_{at}, only at distances from $\mathbf{r} = 0$ to a distance of the order of the lattice constant. If this is the case, $\psi_n(\mathbf{r})$ will be an excellent approximation to a stationary-state wave function for the full crystal Hamiltonian, with energy eigenvalues being equal to the energy of the atomic level, E_n. However, to study more complex systems, such as carbon and silicon structures, where all the electrons are not well localized in the neighborhood of each lattice point, we need to make corrections to this extreme case. Therefore, the crystal Hamiltonian can be approximated as

$$H = H_{at} + \Delta U(\mathbf{r}), \tag{2.29}$$

where $\Delta U(\mathbf{r})$ is the correction to the atomic potential to produce the full periodic Hamiltonian of the crystal from the atomic Hamiltonian. In other words, the bound level of the atomic Hamiltonian, $\psi_n(\mathbf{r})$, which satisfies the atomic Schrödinger equation Eq. (2.28), will also satisfy the crystal Schrödinger equation, provided that the correction term $\Delta U(\mathbf{r})$ vanishes whenever $\psi_n(\mathbf{r})$ is not small. When this is the case, using $\mathbf{R}$ as a collective index to denote the coordinates of each of the N sites in the lattice, each atomic level $\psi_n(\mathbf{r})$ would yield N degenerate levels in the periodic potential, with wave functions $\psi_n(\mathbf{r} - \mathbf{R})$, for each N sites in the lattice.

According to Bloch's theorem, under a crystal lattice translation which carries $\mathbf{r}$ to $\mathbf{r} + \mathbf{R}$ we have

$$\psi(\mathbf{r} + \mathbf{R}) = e^{i\mathbf{k} \cdot \mathbf{R}}\psi(\mathbf{r}) \tag{2.30}$$

and the N linear combinations of these degenerate wave functions is

$$\psi(\mathbf{r}) = \sum_{\mathbf{R}} e^{i\mathbf{k}\,\cdot\,\mathbf{R}} \psi_n(\mathbf{r}\,-\,\mathbf{R}) \tag{2.31}$$

which satisfies the Bloch condition, Eq. (2.30), with wave vector $\mathbf{k}$, while continuing to display the atomic character of the levels. Furthermore, the crystal Schrödinger equation is

$$H\psi(\mathbf{r}) = (H_{at} + \Delta U(\mathbf{r}))\psi(\mathbf{r}) = \varepsilon(\mathbf{k})\psi(\mathbf{r}), \tag{2.32}$$

where $\varepsilon(\mathbf{k})$ is the energy bands of the crystal. However, when we assume that the solution of the full crystal Schrödinger equation is N linear combinations of degenerate atomic wave functions, Eq. (2.31), $\varepsilon(\mathbf{k})$ is simply equal to the energy of the atomic level, E_n, regardless of the value of $\mathbf{k}$. This deficiency is due to the unrealistic assumption that $\Delta U(\mathbf{r})$ vanishes whenever $\psi_n(\mathbf{r})$ is not small. A more realistic assumption is that $\psi_n(\mathbf{r})$ is small, but not precisely zero, when $\Delta U(\mathbf{r})$ is appreciable. Following this assumption, retaining the general form of the solution, Eq. (2.31), we seek a solution to the full crystal Schrödinger equation that is a linear combination of Wannier functions:

$$\psi(\mathbf{r}) = \sum_{\mathbf{R}} e^{i\mathbf{k}\,\cdot\,\mathbf{R}} \phi(\mathbf{r}\,-\,\mathbf{R}), \tag{2.33}$$

where the Wannier function $\phi(\mathbf{r})$ is not necessarily an exact atomic stationary-state wave function. In fact, whenever the product $\Delta U(\mathbf{r})\psi_n(\mathbf{r})$ is small, we expect the function $\phi(\mathbf{r})$ to be close to the atomic wave function $\psi_n(\mathbf{r})$ or to wave functions which are degenerate with $\psi_n(\mathbf{r})$. Furthermore, the $\psi_n(\mathbf{r})$, localized atomic wave functions, constitute our basis set, and so we can express $\phi(\mathbf{r})$ in the form of a linear combination of them

$$\phi(\mathbf{r}) = \sum_n c_n \psi_n(\mathbf{r}) \tag{2.34}$$

If we multiply the crystal Schrödinger equation, Eq. (2.32), by the atomic wave function $\psi_m^*(\mathbf{r})$ and integrate over all $\mathbf{r}$, we have

$$\int \psi_m^*(\mathbf{r}) H_{at} \psi(\mathbf{r}) d\mathbf{r} + \int \psi_m^*(\mathbf{r}) \Delta U(\mathbf{r}) \psi(\mathbf{r}) d\mathbf{r} = \varepsilon(\mathbf{k}) \int \psi_m^*(\mathbf{r}) \psi(\mathbf{r}) d\mathbf{r}. \tag{2.35}$$

The first term on the right of Eq. (2.35) is simply equal to

$$\int \psi_m^*(\mathbf{r}) H_{at} \psi(\mathbf{r}) d\mathbf{r} = \int (H_{at} \psi_m(\mathbf{r}))^* \psi(\mathbf{r}) d\mathbf{r} = E_n \int \psi_m^*(\mathbf{r}) \psi(\mathbf{r}) d\mathbf{r}. \tag{2.36}$$

Then we find that

$$(\varepsilon(\mathbf{k}) - E_m) \int \psi_m^*(\mathbf{r}) \psi(\mathbf{r}) d\mathbf{r} = \int \psi_m^*(\mathbf{r}) \Delta U(\mathbf{r}) \psi(\mathbf{r}) d\mathbf{r}. \tag{2.37}$$

Finally, using the orthogonality condition for the atomic wave functions

$$\int \psi_m^*(\mathbf{r}) \psi_n(\mathbf{r}) d\mathbf{r} = \delta_{nm} \tag{2.38}$$

and substituting (2.33) and (2.34) into (2.37), we arrive at an eigenvalue equation that determines the band energies $\varepsilon(\mathbf{k})$ and coefficients c_n:

$$\begin{aligned}
(\varepsilon(\mathbf{k}) - E_m) c_m &= -(\varepsilon(\mathbf{k}) - E_m) \sum_n \{ \sum_{\mathbf{R} \neq 0} \int \psi_m^*(\mathbf{r}) \psi_n(\mathbf{r} - \mathbf{R}) e^{i\mathbf{k}.\mathbf{R}} d\mathbf{r} \} c_n \\
&+ \sum_n \{ \sum_{\mathbf{R} \neq 0} \int \psi_m^*(\mathbf{r}) \Delta U(\mathbf{r}) \psi_n(\mathbf{r} - \mathbf{R}) e^{i\mathbf{k}.\mathbf{R}} d\mathbf{r} \} c_n \\
&+ \sum_n \{ \int \psi_m^*(\mathbf{r}) \Delta U(\mathbf{r}) \psi_n(\mathbf{r}) d\mathbf{r} \} c_n
\end{aligned} \tag{2.39}$$

where $\Delta U(\mathbf{r})$ is the deviation of the full periodic crystal potential from the atomic potential.

The third term on the right of Eq. (2.39) contains the product $\Delta U(\mathbf{r}) \psi_n(\mathbf{r})$. We interpret our assumption of well localized atomic levels to mean that $\Delta U(\mathbf{r}) \psi_n(\mathbf{r})$ is small because we expect the atomic wave functions $\psi_n(\mathbf{r})$ to become small at distances large enough for the deviation $\Delta U(\mathbf{r})$ to be appreciable. Consequently, following our assumption of well localized atomic levels, it is clear that the second term is small. In

addition, the integrals in the first and second terms on the right of Eq. (2.39), whose integrands contain the product of two atomic stationary-state wave functions centered at different lattice sites, are called *overlap integrals*. The orthogonality condition for the atomic wave functions, Eq. (2.38), says that two atomic wave functions are orthogonal if they are bound levels of the Hamiltonian of the same atom. In other words, atomic wave functions are associated with the atomic orbitals and they are orthogonal if the orbitals are on the same atom. It is not true, obviously, if the orbitals are on different atoms. As a matter of fact, it is precisely the overlap of the orbitals on different atoms which creates the bond between the carbon and silicon atoms.

Clearly, to solve the eigenvalue equation, Eq. (2.39), and determine the band energies of the full crystal at each molecular dynamics simulation time step will require the evaluation of overlap integrals and computational workload increases accordingly. Therefore, there is a clear need to make a number of approximations in order to simplify the integrals but retain the molecular orbital description. In fact, the tight binding approximation deals with the case in which the atomic description is not completely irrelevant but the overlap of atomic wave functions require corrections to the picture of isolated atoms. In other words, overlap integrals are generally small and the tight binding approximation exploits the smallness of these integrals. The tight binding method eliminates these difficult integrals and includes them in the eigenvalue equation, Eq. (2.39), as parameters that have been fitted to reproduce some properties of the system that are determined either from experimental data or from first principles calculations.

To simplify the eigenvalue equation, Eq. (2.39), and to keep the tight binding parameters as low as possible, we make another approximation. The second approximation is to express the solution to the full crystal Schrödinger equation in the form of a linear combination of bound levels of a single isolated atom. In other words, the basis set is derived from the atomic Hamiltonian which is assumed to be the same as the molecular electronic Hamiltonian for an isolated atom. Mathematically we can write electronic states of one electron moving in an average field due to the other

electrons and ion cores as

$$H\psi_i = E_i\psi_i, \tag{2.40}$$

where H is the reduced one-electron Hamiltonian, ψ_i is its ith eigenfunction and E_i is the corresponding energy. In addition, we can write the one electron states of an atomic Hamiltonian as

$$H_\alpha\phi_\alpha = \epsilon_\alpha\phi_\alpha, \tag{2.41}$$

where H_α is the one electron atomic Hamiltonian, and ϕ_α, ϵ_α refer to the one electron atomic orbital and the energy of the single particle state in the atomic picture, respectively. (For an isolated atom, this is an exact expression.) In the tight binding formulation, the ϕ_α constitute our basis set and so we express the molecular orbitals in the form of a linear combination of them

$$\psi_i = \Sigma_\alpha c_{i\alpha}\phi_\alpha \tag{2.42}$$

Operating on molecular orbitals with the molecular electronic Hamiltonian, H, we get

$$H\psi_i = H(\Sigma_\alpha c_{i\alpha}\phi_\alpha) = E_i\psi_i. \tag{2.43}$$

Rewriting Eq. (2.42) in Dirac notation

$$H|i\rangle = \Sigma_\alpha c_{i\alpha}H|i\rangle = E_i|i\rangle, \tag{2.44}$$

we can express the corresponding energy as

$$E_i = \Sigma_{\alpha,\beta}c^*_{\beta i}c_{i\alpha}\langle\beta|H|\alpha\rangle. \tag{2.45}$$

Clearly, the second approximation is simply assuming that the molecular electronic Hamiltonian, H, acts on the atomic orbitals as

$$H|\alpha\rangle = H_\alpha|\alpha\rangle = \epsilon_\alpha|\alpha\rangle \tag{2.46}$$

Beforehand we stated the orthogonality condition for atomic orbitals. In our tight binding formulation atomic orbitals, ϕ_α, introduced in Eq. (2.41), constitute our basis set and we have assumed that ϕ_α and ϕ_β are orthogonal, i.e., that $\langle\alpha|\beta\rangle = \delta_{\alpha\beta}$,

which is true only if the orbitals are on the same atom. (In this thesis, sp^3 basis set is used for carbon and silicon, i.e. we have used the minimal basis of one s and three p orbitals per carbon or silicon atom.) Finally, as a consequence of the second approximation, we note that $\langle\beta|H|\alpha\rangle = 0$ for α, β on the same atom.

The third approximation of the tight binding method deals with the interactions between atoms, especially between atomic orbitals, in the molecular structure. The tight binding overlap parameters, which are included in the eigenvalue equation (2.43) to replace overlap integrals, are restricted to the first neighbor shells of the structures. In other words, only two-center integrals are taken into account, i.e. $\langle\beta|H|\alpha\rangle = 0$ for α, β on distant atoms and $\langle\beta|H|\alpha\rangle \neq 0$ for α, β on nearest neighbor atoms. Undoubtedly, this approximation leads to a great simplification to the eigenvalue equation (2.43) and the tight binding Hamiltonian, which will be discussed in more detail in the next chapter.

In general, of course, $\langle\beta|H|\alpha\rangle$ has to depend on the interatomic separation [25]. In the tight binding model, however, $\langle\beta|H|\alpha\rangle$ are parameters which are calculated for the nearest neighbor separation in the equilibrium structure and then allowed to vary according to a distance dependent scaling function. The final approximation of the tight binding model is that short-ranged interactions are assumed. In the next chapter, the consequences of this assumption will be discussed in detail and the short-ranged scaling functions used in this thesis will be introduced. In addition, suggested pairwise potentials and short-ranged effective repulsive potentials will be introduced.

Chapter 3

METHODOLOGY

In 1989 Goodwin, Skinner and Pettifor (GSP) presented a novel method of obtaining transferable tight binding (TB) parameters and applied it to silicon [27]. The lowest energy geometries obtained by Goodwin *et al* using the TB molecular dynamics method agree with those found by using accurate *ab initio* molecular orbital techniques. A transferable TB model for silicon is found by fitting the energies of silicon in various bulk crystal structures and examining the functional parametrizations of the TB forms. The functional forms suggested by Goodwin *et al* for the hopping parameters and pairwise potential are introduced in this chapter.

In the GSP model, the TB parameters were restricted to the first neighbor shells of the structures [27]. However, Kwon *et al* [24] have argued that it is impossible to choose a unique cutoff distance in the GSP tight binding model that satisfies the condition that all crystalline structures of silicon have only nearest neighbor interactions. They addressed the problem of the GSP model in Ref. [24] and examined alternative scaling forms for the hopping parameters that can be used with a single unique cutoff distance in molecular dynamics simulation studies of different crystalline silicon structures. They started with the GSP tight binding model and allowed greater functional freedom to provide a better fit to the bulk silicon crystal structures. We do not discuss their strategy and refer to the paper [24]. The resulting set of tight binding parameters suggested by Kwon *et al* are listed and the deficiencies of their model when applied to SW silicon hexagonal nanotubes (h-NTs) will be discussed in the rest of the chapter.

Xu *et al* [23] developed for carbon a similar TB interatomic potential in which they adopted the scaling form given by Goodwin *et al* for the dependence of the TB

hopping parameters and the pairwise potential on the interatomic separation. Their TB model for carbon has shown to have good transferability when applied to a wide variety of carbon structures. The parameters for the scaling forms in their model are chosen primarily by fitting first principles or *ab initio* results of energy versus nearest neighbor interatomic separation for different carbon structures with special emphasis on the diamond and graphite. The set of TB parameters suggested by Xu *et al* reproduced excellently the energy curves of the two structures [23], i.e. graphite and diamond (See Fig. 1 of Ref [23]).

A single wall carbon nanotube is basically described as a graphene sheet (a single layer of graphite) rolled into a cylindrical shape so that the structure is one dimensional with axial symmetry. Since the set of TB parameters for carbon suggested by Xu *et al* is transferable to the graphene structure [23], Dereli *et al* [18] [19] [20] adopted these parameters in optimizing single wall carbon nanotube using TBMD simulations. Dereli *et al* bent the graphene sheet and periodic boundary conditions were imposed in axial direction along the tube and free boundary conditions in the radial direction. So effectively an isolated SW carbon NT were simulated [18] [19] [20] to investigate their physical properties using TBMD method adopted from L. Colombo [25]. The TBMD scheme and the design of the computational tools will be discussed in the next sections.

It is known that graphite is a stable structure for carbon, whereas for silicon diamond structure is the most stable [1]. In other words, the sp^2 hybridization is more stable in carbon, whereas the sp^3 hybridization is more stable in silicon. However, despite the difficulties having an sp^2-like (graphenelike) structure for silicon, many researchers do not completely rule out the possibility of the existence of single wall (SW) silicon h-NTs, i.e. silicon nanotubes with the structures of carbon nanotubes. In the literature, two types of silicon nanotubes are studied using *ab initio* calculations: SW silicon hexagonal nanotubes (h-NTs) [2] [4] [5] [7] [8] [9] [10] [11] [12] [13] and SW silicon gear-like nanotubes (g-NTs) [5] [6] [7]. As introduced in the first chapter, SW silicon g-NTs and h-NTs are formed by rolling the (111) sheet of the silicon diamond

structure and silicon graphenelike sheet, respectively [5]. In this thesis, we studied SW silicon h-NTs using the same strategy that Dereli *et al* [18] [19] [20] developed for SW carbon nanotube TBMD simulations. In our studies, silicon h-NT structures are constructed by folding a graphenelike sheet of silicon into a cylindrical shape. The periodic boundary conditions are applied along the axial direction of the tube.

Aforementioned, Kwon *et al* [24] have presented a TB model for silicon that accurately describes the behavior of silicon in crystalline phases. However, their model does not give the energy curves of the hexagonal silicon graphenelike sheets. Using the results of the *ab initio* studies of silicon graphenelike sheet [4] and SW silicon h-NTs, we first determined the position of the energy curves for the graphenelike silicon sheet structures or namely SW silicon h-NTs, i.e. energy versus nearest neighbor interatomic separation. Fagan *et al* [4] found that the silicon graphenelike sheet has a total energy per atom value of 0.79 eV higher than the total energy per atom for the silicon in the crystal structure. They also noted that the nearest neighbor interatomic separation is found to be $2.25\mathring{A}$ at equilibrium structure. Once we have determined the position of the energy curve for the silicon graphenelike sheet structure or namely SW silicon h-NTs, we extracted the set of TB potential parameters from the results of the *ab initio* [4] calculations using a nonlinear least-squares fitting routine. We present our basic strategy to extract the TB parameters in Section 3.2.

Before we present the results of our TBMD simulation studies of SW silicon h-NTs in Chapter 4, this chapter offers an overview of the methods employed in this thesis. In Section 3.1 we introduce our TBMD scheme which is presented by L. Colombo [25] and adopted for SWCNT TBMD simulation studies by Dereli *et al* [18] [19] [20], introduce the functional forms suggested by Goodwin *et al* [27] for the hopping integrals and pair potentials and finally introduce the set of TB potential parameters suggested by Xu *et al* [23] and Kwon *et al* [24] for carbon and silicon respectively. The method that we have used to find the appropriate potential parameters for silicon graphenelike sheet structures or SW silicon h-NTs from the *ab initio* results will be presented in Section 3.2. Finally in Section 3.3 we present the method that we have

adopted for computing the total forces on nuclei at each MD step.

3.1 TB Matrix and Parametrizations

In order to calculate the electronic structure of a molecular system using the TB model, we start with the many body Hamiltonian of the system written in the adiabatic approximation. But the TB model assumes that the total Hamiltonian can be simplified into a series of reduced one electron Hamiltonians [25], [28] i.e. that each electron feels an average field made up of the nuclei and all other electrons. Furthermore, single particle wave functions are represented as a linear combination of atomic orbitals, i.e. $\psi_n = \Sigma_i c_i^n \phi_i$, where ψ_n is the nth single particle wave function and the set of atomic orbitals $\{\phi_i\}$ is our basis set. Finally, the energy eigenvalues of the single particle states are found by solving the Schrödinger equation

$$(H_{ij} - \epsilon_n S_{ij}) c_i^n = 0 \tag{3.1}$$

where ϵ_n is the nth eigenvalue and c_i^n is the ith component of the nth eigenvector. And we have

$$H_{ij} = \langle \phi_i | H | \phi_j \rangle \tag{3.2}$$

$$S_{ij} = \langle \phi_i | \phi_j \rangle \tag{3.3}$$

where the indices i and j run over all the basis elements, i.e. atomic orbitals. For an orthogonal basis set, S_{ij} is simply a unit matrix. When the basis set is a set of atomic orbitals, $S_{ij} = 0$ only if orbitals are on the same atom, however it is not true if the orbitals are on different atoms. Therefore, for the non-orthogonal basis set, the overlap integrals $\int \phi_i \phi_j d\mathbf{r}$ must be calculated explicitly. The evaluation of overlap integrals causes a high computational workload [25] [18] [19] [20]. However it is possible to define an orthogonal set of orbitals, which are known as Löwdin orbitals. Hypothetical basis orbitals are centered around each ion with the same angular symmetries of single atom eigenstates. In other words, the non-orthogonality of basis orbitals is neglected and a new orthogonal basis set is defined. Now we

have $S_{ij} = \delta_{ij}$. Furthermore, in order to represent the $|\phi_i\rangle$ basis orbitals in a more convenient way, we use two labels, i.e. $|\phi_{l\alpha}\rangle$, where α refers to the ion around which the orbital is centered and l is the quantum number index referring to the orbital type. The energy eigenvalue equation finally reduces to

$$(\langle\phi_{l\alpha}|H|\phi_{l'\alpha'}\rangle - \epsilon_n\delta_{ll'}\delta_{\alpha\alpha'})c^n_{l\alpha} = 0 \tag{3.4}$$

It is clear that in a system consisting of n atoms with Z valance electrons per atom, the electronic Hamiltonian matrix, $\langle\phi_{l\alpha}|H|\phi_{l'\alpha'}\rangle$, of dimension $nZ \times nZ$ will be constructed at each time step of the simulation. Within our semi-empirical TB model, we make a number of simplifications to the electronic Hamiltonian matrix. The elements of the Hamiltonian matrix are evaluated by fitting a suitable database obtained either from experiments or by first principles methods. In this thesis, sp^3 basis set is used for the carbon and silicon structures, i.e. one s and three p orbitals per atom. Consequently, the diagonal elements of the electronic Hamiltonian matrix are simply the atomic orbital energies of the corresponding atom labeled by α. For carbon and silicon molecular systems, the diagonal elements of the matrix $\langle\phi_{l\alpha}|H|\phi_{l'\alpha'}\rangle$ are E_s and E_p, which are adjusted so that an isolated carbon or silicon atom in the ground state is at zero energy. These are [23], [24]:

Atomic orbital energies	Carbon	Silicon
E_s (eV)	-2.99	-5.25
E_p (eV)	3.71	1.20

In addition, the off-diagonal elements of the electronic Hamiltonian matrix correspond to the hopping integrals between atoms. They are simply described by a set of orthogonal sp^3 two-center hopping parameters h_γ, where γ denotes the four tight-binding overlaps, $ss\sigma$, $sp\sigma$, $pp\sigma$, $pp\pi$. The hopping parameters for carbon and silicon are well known [23], [24]:

Hopping Parameters	Carbon	Silicon
$h_{ss\sigma}(r_0)$ (eV)	-5.0	-2.038
$h_{sp\sigma}(r_0)$ (eV)	4.7	1.745
$h_{pp\sigma}(r_0)$ (eV)	5.5	2.750
$h_{pp\pi}(r_0)$ (eV)	-1.55	-1.075

In general, of course, the hopping parameter h_γ has to depend on the interatomic distance, and our model does that. In our TB model, h_γ is calculated for fixed interatomic distances, and then is allowed to vary according to a scaling function $s_\gamma(r)$ as

$$h_\gamma(r) = h_\gamma(r_0)s_\gamma(r) \tag{3.5}$$

where $h_\gamma(r_0)$ is the tight-binding overlap at the fixed nuclei geometry. Here, r_0 denotes the nearest neighbor atomic separation in the equilibrium structure. Furthermore, the functional form suggested by Goodwin *et al* [27] for the scaling function that we have adopted in our calculations is

$$s_\gamma(r) = (\frac{r_0}{r})^n \exp\{n[-(\frac{r}{r_{c\gamma}})^{n_{c\gamma}} + (\frac{r_0}{r_{c\gamma}})^{n_{c\gamma}}]\} \tag{3.6}$$

where r_0 is the nearest neighbor atomic separation. For the parameters n, $n_{c\gamma}$ and $r_{c\gamma}$ see the reference papers [23], [24].

Once we construct the electronic Hamiltonian matrix, we can simply obtain the electronic band structure energy E_{bs} by diagonalizing the TB matrix, and thereby summing over all the single electron energy eigenvalues [25]:

$$E_{bs} = \sum_n \epsilon_n f(\epsilon_n, T) \tag{3.7}$$

where $f(\epsilon_n, T)$ is the Fermi-Dirac distribution. In addition, the effective repulsive potential E_{rep} due to the interactions among ion cores can be expressed as a sum of appropriate pair potentials:

$$E_{rep} = \sum_\alpha f[\sum_\beta \phi(r_{\alpha\beta})] \tag{3.8}$$

Then the total energy of the molecular system with ion cores and valance electrons can be written as

$$E_{total} = E_{bs} + E_{rep}. \tag{3.9}$$

In Eq. (3.8), $\phi(r_{\alpha\beta})$ is the appropriate pair potential between atoms α and β, which is in the form suggested by Goodwin *et al* [27]. In addition, f is a functional expressed as a 4th order polynomial.

$$\phi(r) = \phi_0(\frac{d_0}{r})^m \exp\{m[-(\frac{r}{d_c})^{m_c} + (\frac{d_0}{d_c})^{m_c}]\} \tag{3.10}$$

$$f(x) = \sum_{n=0}^{4} C_n x^n \tag{3.11}$$

where x is the sum of the pair potentials from the neighbors of an atom.

3.2 TB Potentials for Carbon and Silicon

In the suggested forms of the pair potential $\phi(r)$ and scaling functions $s_\gamma(r)$ for both carbon [23] and silicon [24] molecular systems, short-range interactions are assumed and only the nearest neighbor interactions are taken into account. Therefore, the coefficients in Eq. (3.10) and Eq. (3.6) are determined by requiring that $\phi(r)$ and $s_\gamma(r)$ go smoothly to zero at the cutoff distance, which is between the nearest neighbor and the next nearest neighbor distance of carbon or silicon atoms in the SW carbon NTs and silicon h-NTs. The parameters for the two-body pair potentials $\phi(r)$ and the coefficients of the functional $f(x) = \sum_{n=0}^{4} C_n x^n$ that are suggested for carbon and silicon by Xu *et al* [23] and Kwon *et al* [24] are

Two-body parameters	Carbon (Ref. [23])	Silicon (Ref. [24])
m	3.30304	6.8755
m_c	8.6655	13.017
d_c (Å)	2.1052	3.66995
d_0 (Å)	1.64	2.36
C_0 (eV)	-2.5909765	0
C_1 (eV)	0.5721151	2.1604385
C_2 (eV)	$-1.7896349 \times 10^{-3}$	-0.1384393
C_3 (eV)	2.3539222×10^{-5}	5.8398423×10^{-3}
C_4 (eV)	$-1.2425117 \times 10^{-7}$	$-8.0263577 \times 10^{-5}$

Aforementioned the TB model presented by Xu *et al* [23] for carbon is transferable to the graphene structure and the results that Dereli *et al* [18] [19] [20] have obtained by adopting this model in TBMD simulation studies of SWCNTs are in good agreement with those obtained from *ab initio* calculations. However, the TB model presented by Kwon *et al* [24] for silicon does not give the energy curve of the hexagonal silicon graphenelike sheets. Using a nonlinear least-squares fitting routine, we determined the set of TB potential parameters for silicon graphenelike sheet structures or SW silicon h-NTs from the results of the *ab initio* calculations [4].

For the convenience of molecular dynamics simulation, we require the pair potential $\phi(r)$ and scaling functions $s_\gamma(r)$ to go smoothly to zero at some designated cutoff distance. In our TB model for silicon h-NTs, we choose a cutoff distance of $3.6\mathring{A}$. Indeed, the scaling functions $s_\gamma(r)$ for the TB hopping matrix elements go to zero smoothly at $3.6\mathring{A}$ (See Fig. 1 of Ref [24]). Therefore, our basic strategy is as follows: For the set of tight binding parameters (h_γ, n r_0, $r_{c\gamma}$, and $n_{c\gamma}$) suggested by Kwon *et al* [24] the energies of the silicon h-NT are fitted to the *ab initio* results with a nonlinear least-squares fitting routine to extract values for the two-body functional parameters (ϕ_0, d_0, d_c, m, and m_c, C_n). Fagan *et al* [4] found that the silicon graphenelike sheet has a total energy per atom value at $T = 0K$ of 0.79 eV higher than the total energy per atom for the silicon in the crystal structure. They also obtained a number of

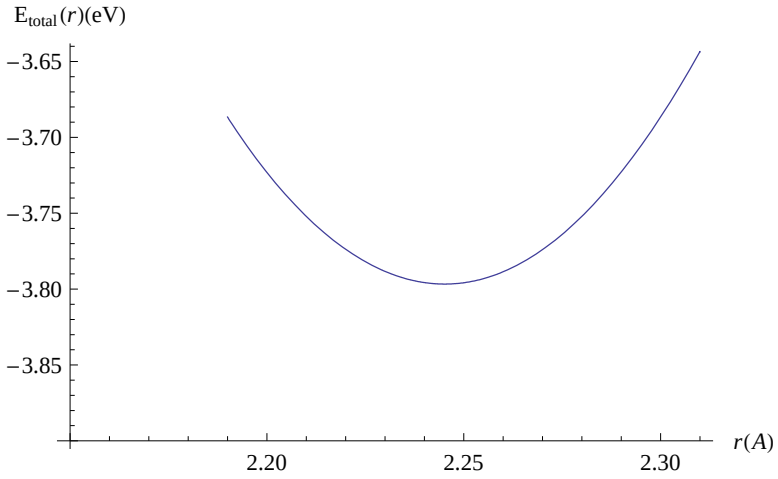

Figure 3.1: Total energy E_{tot} per atom of silicon in the (10,0) SW silicon h-NT structure as a function of nearest neighbor distance r. The position and the shape of the curve is determined from the results of the *ab initio* calculations [4] and using the analogy between SW carbon NTs and SW silicon h-NTs.

the order of 0.04 eV/atom to curve the sheets into a cylinder to form a silicon (10,0) h-NT. In addition, they reported that the nearest neighbor distances for the (10,0) h-NT at equilibrium is around $2.245\mathring{A}$ [4]. From their results and using the analogy between SW carbon NTs and SW silicon h-NTs we determined the position and the shape of the energy curve for (10,0) SW silicon h-NT. Finally, we concluded that once we determine the band structure energy per atom value for (10,0) silicon h-NT, the repulsive energy contribution to the total energy can be obtained by subtracting the the band structure energy from the calculated $T = 0K$ total energy/atom.

TB hopping matrix elements h_γ are scaled properly for silicon graphenelike sheet and silicon h-NTs in the TB model suggested by Kwon *et al* [24], i.e. they smoothly go to zero at the designated cutoff $3.6\mathring{A}$ which is between the first neighbor and the next nearest neighbor distance. Therefore the TB parameters required for describing the electronic structure of silicon h-NTs are obtained from Kwon's work on the TB model for silicon. These parameters (h_γ, n r_0, $r_{c\gamma}$, and $n_{c\gamma}$) are introduced in Section 3.1. We have calculated the band structure energy of silicon (10,0) h-NT using these

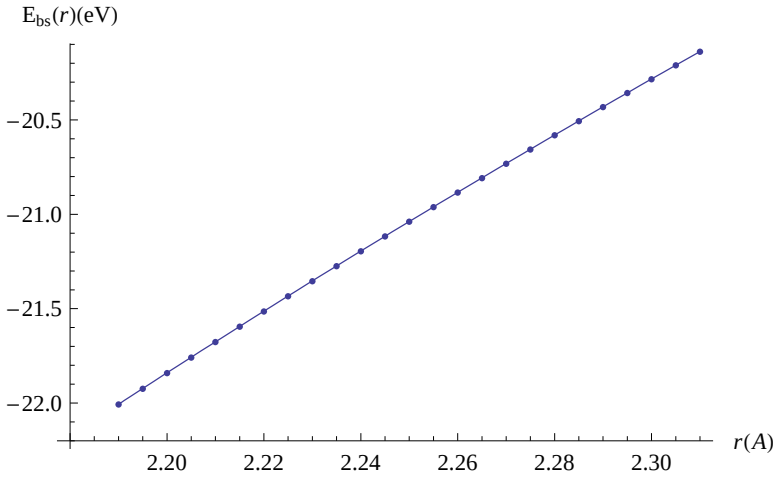

Figure 3.2: Band structure energy E_{bs} per atom of silicon in the (10,0) silicon h-NT structure as a function of nearest neighbor distance r. The circles are the results of the semi-empirical TB calculation using the TB parameters suggested by Kwon *et al* [24]; the solid line is the fitting third order polynomial function.

parameters at various interatomic separations and we have obtained the band structure energy function $E_{bs}(r)$. Then we have determined the repulsive energy function $E_{rep}(r)$ by subtracting the band structure energy function $E_{bs}(r)$ from the *ab initio* [4] calculated total energy function $E_{tot}(r)$, i.e.,

$$E_{rep}(r) = E_{total}(r) - E_{bs}(r) \tag{3.12}$$

Finally, the resulting repulsive energy function $E_{rep}(r)$ is fitted with a nonlinear least-square fitting routine to the functional form $E_{rep} = \sum_\alpha f[\sum_\beta \phi(r_{\alpha\beta})]$. Unlike the GSP model, repulsive energy is not a sum of pair potential $\phi(r_{\alpha\beta})]$ in our model. The repulsive energy is a sum of a functional f of the pair potential $\phi(r_{\alpha\beta})]$, similar to the expressions in the TB models of Xu *et al* [23] and Kwon *et al* [24]:

$$\phi(r) = \phi_0(\frac{d_0}{r})^m \exp\{m[-(\frac{r}{d_c})^{m_c} + (\frac{d_0}{d_c})^{m_c}]\} \tag{3.13}$$

$$f(x) = \sum_{n=0}^{4} C_n x^n \tag{3.14}$$

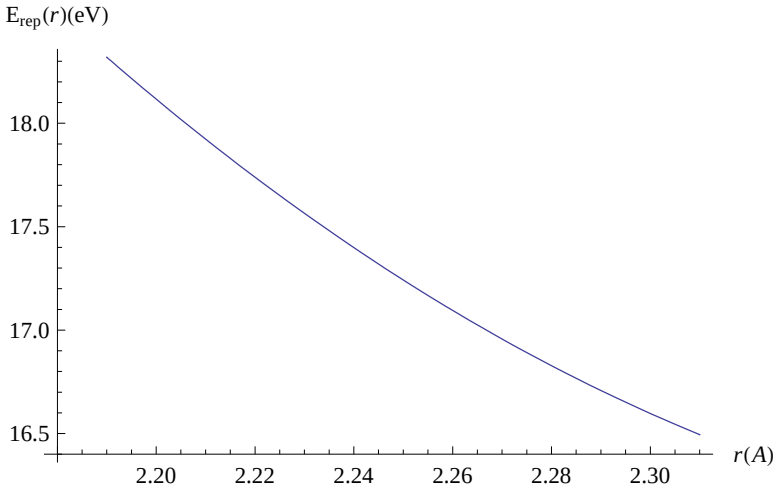

Figure 3.3: Repulsive energy E_{rep} per atom of silicon in the (10,0) SW silicon h-NT structure as a function of nearest neighbor distance r obtained by subtracting $E_{bs}(r)$ from the total energy function $E_{total}(r)$

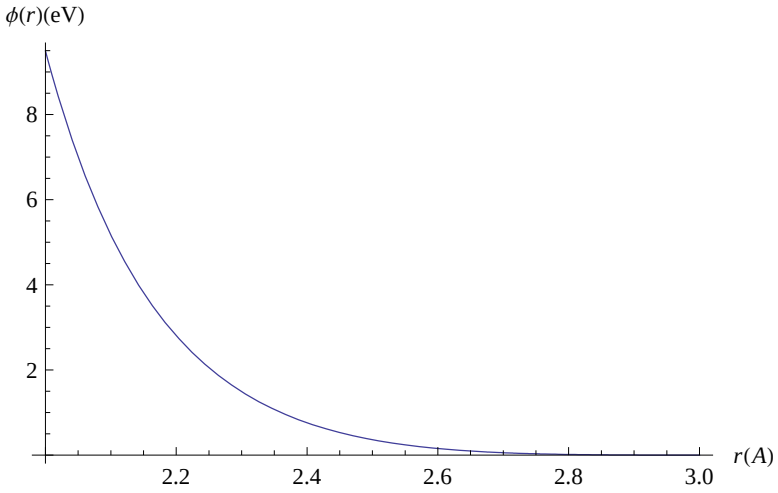

Figure 3.4: Radial dependence of the repulsive pair potential $\phi(r)$ as a function of separation r between atoms, as given by Eq. (3.13)

In our fitting we required that $\phi(r)$ go smoothly to zero at the cutoff distance, which is between the nearest neighbor and the next nearest neighbor distance silicon atoms in the SW silicon h-NTs. The repulsive pair potential $\phi(r)$ and the embedding energy function are plotted in figures 3.4 and 3.5.

Our work on SW carbon NTs with various chiralities using the tight binding model presented by Xu *et al* [23] for carbon have shown that the band structure energy governs the total energy of the tube. For SW carbon NTs with different layer values and chiralities we have obtained similar values for the repulsive energy per atom. It is well known that the equilibrium nearest neighbor distances for the SW carbon NTs with different chiralities are around $1.42\mathring{A}$ [1]. As long as the SW carbon NT remains stable with small fluctuations from the equilibrium structure, the repulsive energy remains the same for each tube structure. It is expected since for a given set of tight binding two-body potential parameters [23] the repulsive energy of the tube depends only on the interatomic separation, which is the same at equilibrium, i.e. $1.42\mathring{A}$, for the SW carbon NTs with different chiralities. Therefore, the position of the total energy curves for different nanotubes are determined by the band structure energy of the tube. (See Fig. 3.6)

Çıracı *et al* [10] reported similar average distances between nearest silicon atoms in SW silicon h-NTs with different chiralities. The nearest neighbor distances for the SW silicon h-NTs are around $2.22\mathring{A}$. Similar to SW carbon NTs, in our tight binding calculations the repulsive energy of SW silicon h-NTs with different chiralities are the same as long as the tubes remain stable. Furthermore the contribution to the forces on each silicon atom due to the repulsive potential energy does not affect the stability of the tube. Following the results obtained by Çıracı *et al* we conclude that the set of tight binding two-body potential parameters that we have found for (10x0) can be used for TBMD simulations of SW silicon h-NTs with different chiralities.

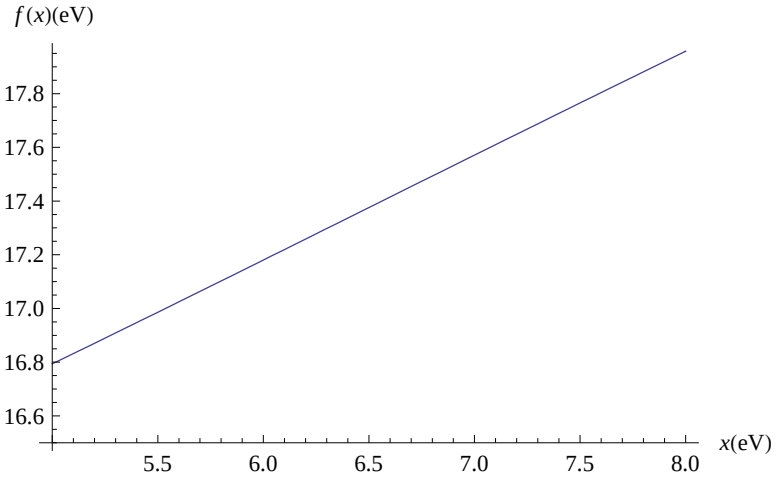

Figure 3.5: The embedding energy function $f(x)$ plotted as a function of x [See Eq. (3.14)]. x is the sum of the pair potentials from the neighbors of an atom.

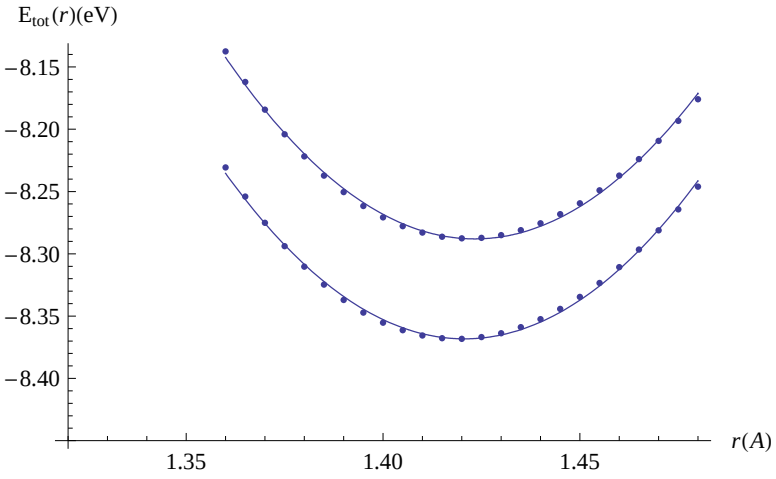

Figure 3.6: Total energy E_{tot} per atom of (10,0) (the upper curve) and (10,10) (the lower curve) SW carbon NTs as a function of nearest neighbor distance r. The circles are the results of the TB calculation using the TB parameters suggested by Xu *et al* [23].

The resulting TB two-body potential parameters for SW silicon h-NTs:

m	11.31
m_c	10.08
d_c (Å)	3.24
C_0 (eV)	15.601913204
C_1 (eV)	-2.810801971 $\times 10^{-2}$
C_2 (eV)	8.394181545 $\times 10^{-2}$
C_3 (eV)	-7.249640335 $\times 10^{-3}$
C_4 (eV)	2.246487249 $\times 10^{-4}$

3.3 Hellmann-Feynman Contribution to the Atomic Forces

For a molecular system in the adiabatic or Born-Oppenheimer approximation, as we discussed in the third section of this chapter, the Hellmann-Feynman theory provides a convenient means to compute the forces on the nuclei. Once we calculate the adiabatic electronic energy eigenvalues of single electron states and thereby the band structure energy of the system by summing energy eigenvalues up to the highest occupied level, we can solve the nuclear dynamics problem using the band structure energy as the adiabatic potential for the nuclei [25].

In addition, the contribution to the total force on the nuclei due to the effective repulsive potential can be trivially calculated. In fact, the repulsive potential is known analytically. (See Section 3.2 and Ref. [23], [24]) Finally, the total force on each of the nuclei is used in the classical molecular dynamics stage of the simulation to update the nuclei positions, velocities and accelerations.

Nuclear motion is governed by the Hamiltonian

$$H_N = T_N + V_n + E_{rep} \tag{3.15}$$

where T_N is the kinetic energy of the nuclei, E_{rep} is the repulsive energy due to nuclear-nuclear interactions, and V_n correspond to the adiabatic potential for the nuclear

motion in the Born-Oppenheimer approximation (See Section 2.3 and Ref. [32], [33], [30]). The forces needed to move nuclei are calculated from the two potential terms, the adiabatic potential V_n and the repulsive potential E_{rep}. The adiabatic potential V_n is equal to

$$V_n = E_{bs} = \sum_n \epsilon_n f(\epsilon_n, T) \tag{3.16}$$

According to the Hellmann-Feynman theory (See Section 2.3 and Ref. [33]), the contribution to the forces on the nuclei due to the adiabatic potential can be obtained by simply calculating the negative gradients of the adiabatic electronic energy eigenvalues. The force acting on the ith nucleus due to the adiabatic potential is

$$\overrightarrow{f}_i = -\frac{\partial}{\partial \overrightarrow{r}_i} \sum_n \epsilon_n f(\epsilon_n, T) = -\sum_n \langle \psi_n | \frac{\partial H}{\partial \overrightarrow{r}_i} | \psi_n \rangle f(\epsilon_n, T) \tag{3.17}$$

where H is the reduced single electron Hamiltonian. The TB approach requires that

$$H\psi_n = \epsilon_n \psi_n \tag{3.18}$$

where ψ_n is the wave function, which describes the nth single electron state and ϵ_n is the corresponding energy eigenvalue. In our TB formulation, the non-orthogonality of basis orbitals is neglected and a new orthogonal basis orbital set $|\phi_{l\alpha}\rangle$ is defined (Löwdin orbitals) [25]. Here l is the quantum number index referring to the orbital type and α labels the ion around which the orbital is centered. Therefore, the single particle wave function is expressed as a linear combination of orthogonal atomic orbitals:

$$\psi_n = \sum_{l\alpha} c^n_{l\alpha} |\phi_{l\alpha}\rangle \tag{3.19}$$

Consequently, we have

$$\langle \psi_n | \frac{\partial H}{\partial \overrightarrow{r}_i} | \psi_n \rangle f(\epsilon_n, T) = \sum_{l\alpha} \sum_{l'\alpha'} c^n_{l'\alpha'} \langle \phi_{l'\alpha'} | \frac{\partial H}{\partial \overrightarrow{r}_i} | \phi_{l\alpha} \rangle c^n_{l\alpha} \tag{3.20}$$

The products $\langle \phi_{l'\alpha'} | H | \phi_{l\alpha} \rangle$ correspond to the elements of the single particle Hamiltonian, i.e. $H_{l\alpha l'\alpha'}$. However, in our TB model, as noted in the previous section, the matrix elements are calculated for fixed interatomic distances and allowed to vary

according to the scaling function $s(r)$. (See Eq. (3.6)) We have

$$H_{l\alpha l'\alpha'}(r_0) = \langle \phi_{l'\alpha'}|H|\phi_{l\alpha}\rangle \tag{3.21}$$

where r_0 is the nearest neighbor separation at the equilibrium structure. Then

$$H_{l\alpha l'\alpha'}(r_{\alpha\alpha'}) = s(r_{\alpha\alpha'})H_{l\alpha l'\alpha'}(r_0) = s(r_{\alpha\alpha'})\langle \phi_{l'\alpha'}|H|\phi_{l\alpha}\rangle \tag{3.22}$$

Finally, the force on the ith nucleus due to the adiabatic potential is given by

$$\begin{aligned}
\overrightarrow{f}_i = -\frac{\partial}{\partial \overrightarrow{r}_i}\sum_n \epsilon_n f(\epsilon_n, T) &= -\sum_n \langle \psi_n|\frac{\partial H}{\partial \overrightarrow{r}_i}|\psi_n\rangle f(\epsilon_n, T) \\
&= -\sum_n f(\epsilon_n, T)\sum_{l\alpha}\sum_{l'\alpha'} c^n_{l'\alpha'}\langle \phi_{l'\alpha'}|\frac{\partial H}{\partial \overrightarrow{r}_i}|\phi_{l\alpha}\rangle c^n_{l\alpha} \\
&= -\sum_n f(\epsilon_n, T)\sum_{l\alpha}\sum_{l'\alpha'} c^n_{l'\alpha'}\frac{\partial H_{l\alpha l'\alpha'}(r_{\alpha\alpha'})}{\partial \overrightarrow{r}_i} c^n_{l\alpha}
\end{aligned} \tag{3.23}$$

where the matrix elements $H_{l\alpha l'\alpha'}(r_{\alpha\alpha'})$ are defined in Eq. (3.21)

In the above derivation we left out the repulsive potential energy function E_{rep}. Since it is known analytically, the forces due to E_{rep} can be calculated straightforwardly. To find the total force on the ith nucleus, the contribution due to the repulsive potential energy, $-\frac{\partial E_{rep}}{\partial \overrightarrow{r}_i}$, is trivially added to the Hellmann-Feynman forces.

Chapter 4

RESULTS AND DISCUSSION

In our calculations, we have used the TBMD algorithms involving the above mentioned two-body potential parameters together with the tight binding parameters for band structure energy calculations adopted from the work of Kwon *et al* [24]. All the simulations presented in this work are carried out in the canonical (NVT) ensemble. A periodic boundary condition is applied in the axial direction. The Newtonian equations of motion are integrated using the velocity Verlet algorithm with a time step equal to 1 fs. To avoid an inaccurate integration, the velocities of the constituent atoms are occasionally rescaled to maintain the temperature of the system at the target value. Before starting the production phase of the simulations, a careful study of the time step is done. In our simulations studies, we have chosen the time step to be 1 fs, which is adequate and widely used in simulations of atomic motions.

Our results show that the total energy per atom decreases with increasing diameter both for the armchair and zigzag silicon h-NTs. To reveal the structural and energetic features of silicon h-NTs, we have studied various tubes with different diameters and chiralities. Chirality, radius and the calculated total energy per atom value are given in tabular form below for each silicon h-NT that we have studied in this thesis.

Type	Chirality	Radius (Angstroms)	Total Energy / Atom (eV)
zigzag	(4,0)	2.54025503	-3.633640722
zigzag	(5,0)	3.14582542	-3.697235337
zigzag	(6,0)	3.75595820	-3.740119148
zigzag	(8,0)	4.98288949	-3.775546569
zigzag	(9,0)	5.59817862	-3.786355265
zigzag	(10,0)	6.21419018	-3.794399753
zigzag	(13,0)	8.06487713	-3.808708760
zigzag	(17,0)	10.5357191	-3.817373606
armchair	(3,3)	3.26570374	-3.702285770
armchair	(5,5)	5.38914145	-3.783077559
armchair	(6,6)	6.45606254	-3.797763123
armchair	(7,7)	7.52442725	-3.806600907
armchair	(8,8)	8.59368655	-3.812328984
armchair	(9,9)	9.66353901	-3.816251426
armchair	(10,10)	10.7338052	-3.819054244

A. Energetics and Stability

Using TBMD simulation method, we obtained total energy (eV/atom) values for the SW silicon h-NTs with chiralities (6,6), (7,7), (8,8), (10,0) as a function of simulation time. (See figure 4.1) In our calculations, the hexagonal tubes maintain their shape for little disturbance of atoms up to around 3000 MD steps. The bondlengths between neighboring silicon atoms in the nanotube structures, which is $2.245\mathring{A}$, varied little among the nanotubes. Silicon nanotubes are stable around up to 3 ps and then deviations from the ideal structures occur. After 3 ps of equilibration time one atom is detached and the number of detached atoms increases as the simulation proceeds. In Fig. 4.1 sharp peaks after 3 ps of relaxations indicate the detachment of atoms. They are highly metastable structures. In addition, it is observed that small diameter nanotubes collapse more easily.

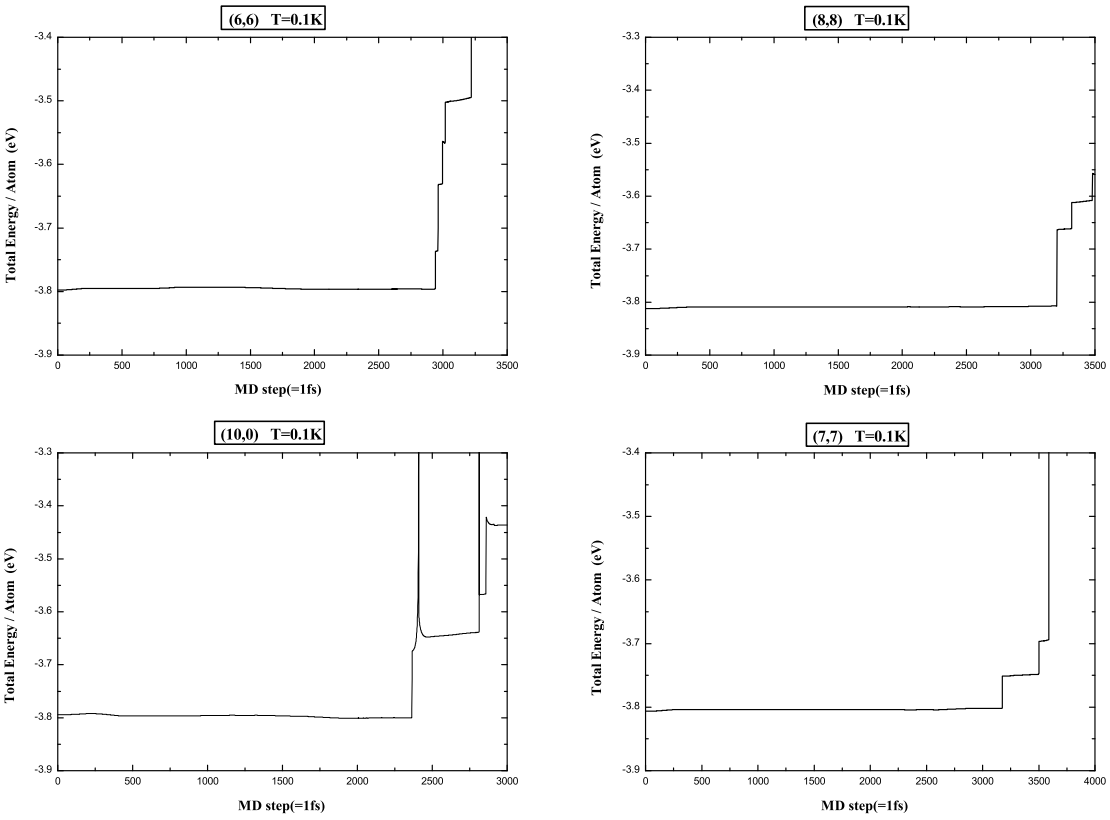

Figure 4.1: Total energy (per atom) for SW silicon h-NTs with chiralities (6,6), (7,7), (8,8), (10,0) as a function of simulation time. Bond breakings between the silicon atoms around $3ps$. The number of detached atoms increases as the simulation proceeds.

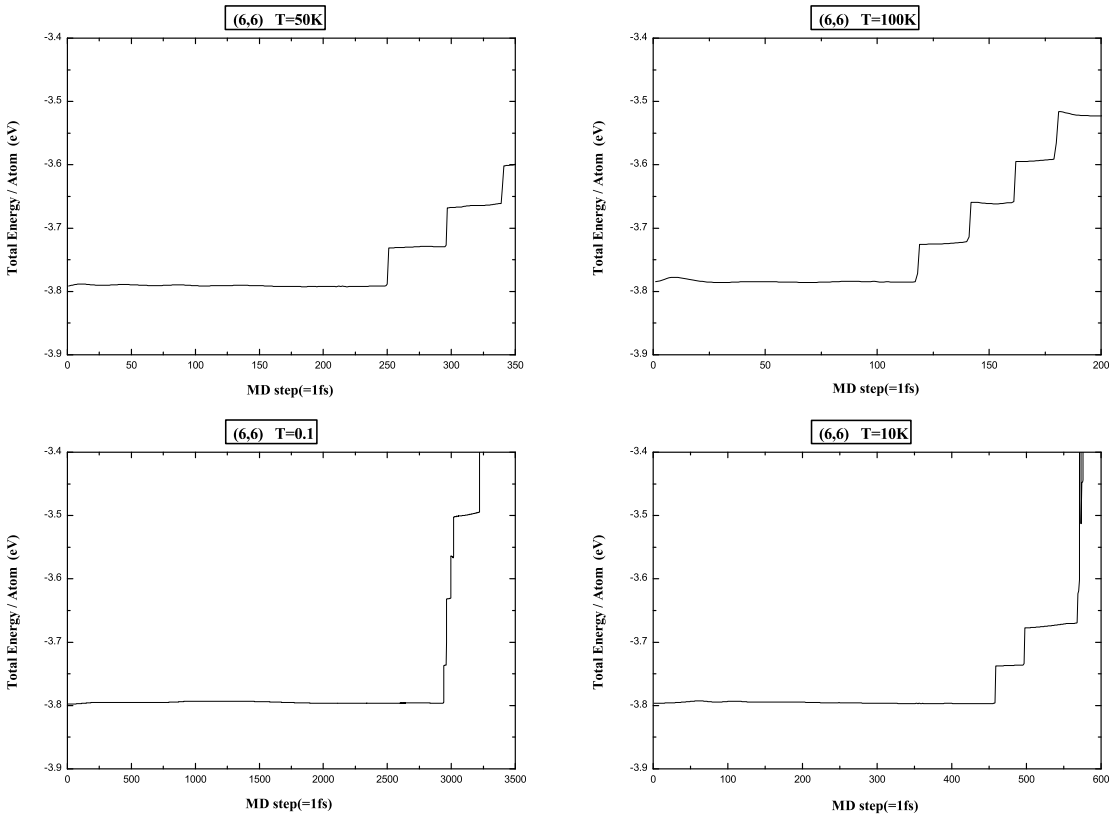

Figure 4.2: Total energy (per atom) for SW (6,6) silicon h-NT as a function of simulation time at various temperatures. As the temperature increases, nanotube collapse more easily.

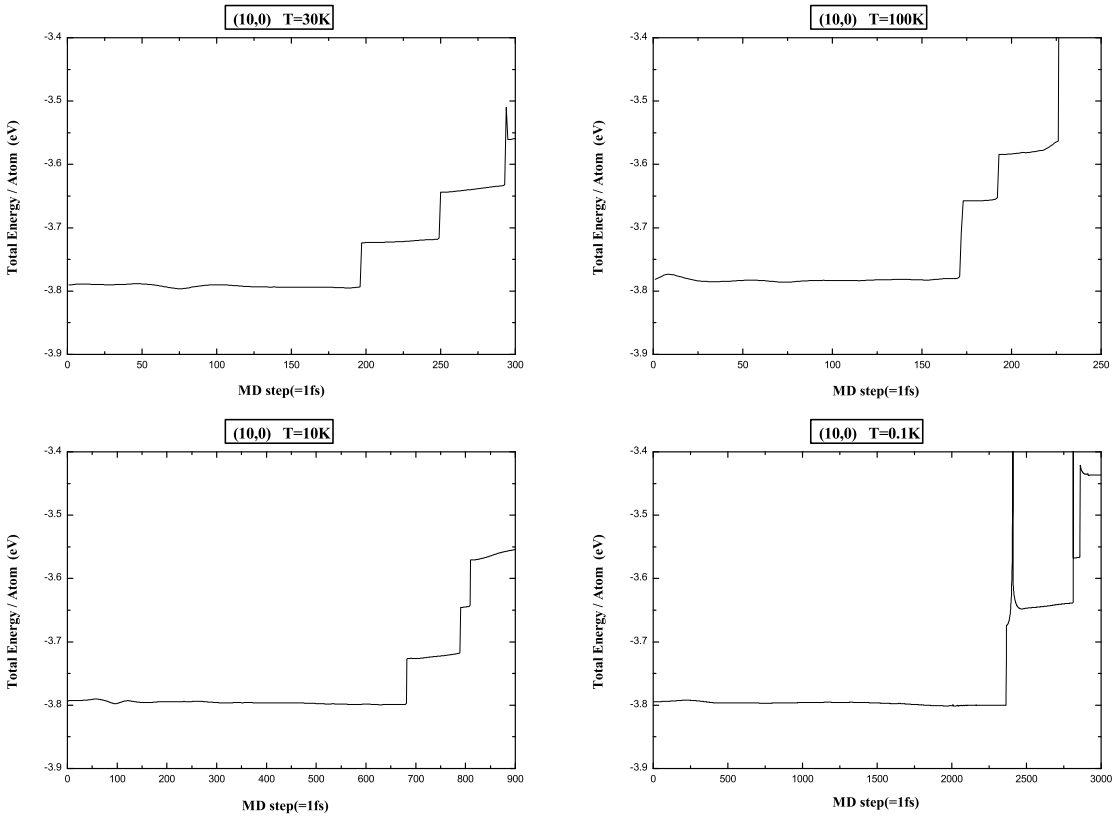

Figure 4.3: Total energy (per atom) for SW (10,0) silicon h-NT as a function of simulation time at various temperatures. As the temperature increases, nanotube collapse more easily.

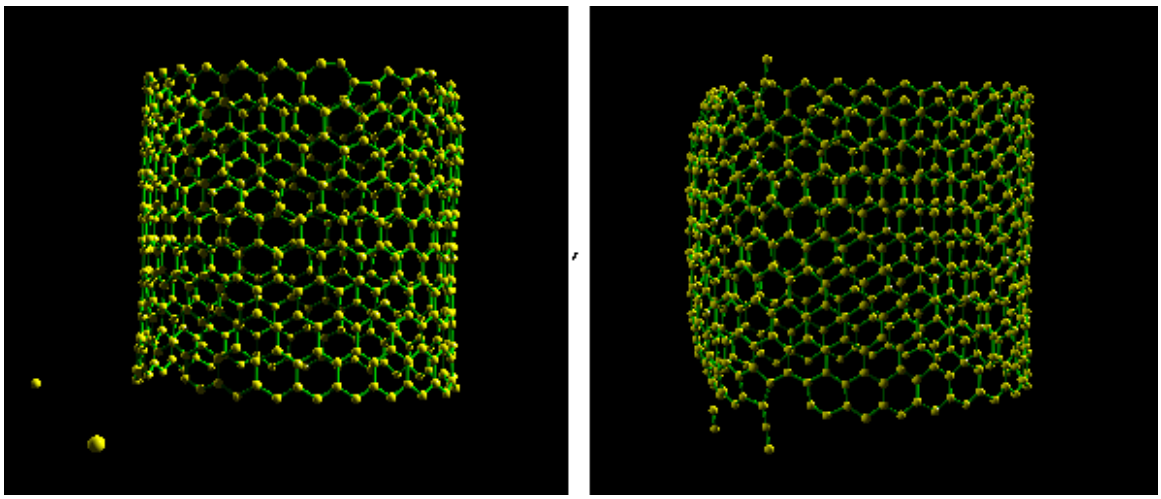

Figure 4.4: Examples of the detachment of atoms during TBMD simulations.

Our predictions about the stability of silicon h-NTs show similar results from Fagan *et al* [4] [11]. Fagan and coworkers explored the possibility of the existence of silicon h-NTs. They emphasized that the energy differences between the total energies per atom for the tubes and the corresponding bulks is much bigger for silicon structures, compared to the carbon structures. This implies the very improbable appearance of a silicon nanotube, namely a single walled silicon h-NT.

Çıracı *et al* reported their analysis of silicon h-NT in [**?**]. The *ab initio* molecular dynamics calculations showed that nanotubes with small diameters transform into clusters even at low temperatures. On the other hand, they reported that silicon nanotubes with relatively large diameters remained stable up to 0.5 ps at higher temperatures up to $800K$. Structural instability of the tubes is enhanced at higher temperatures [10].

To further study the stability of silicon h-NTs, we examined temperature effects. During MD simulations, the position and the velocity of each atom is calculated at each time step. A temperature scale is used

$$\frac{1}{2}mv_i^2 = \frac{3}{2}k_BT \tag{4.1}$$

Temperature affects the structural properties and stability of silicon h-NTs. Temperature effect is examined for the armchair (6,6) and zigzag (10,0) tubes. (Figure 4.2 and Figure 4.3) As the temperature increases, nanotubes collapse more easily. In the temperature range between 0.1-100K, our silicon h-NTs become less stable with increasing temperature. Zhang *et al* [6] found that silicon nanotubes can exist in the structures analogous to those of SWCNTs at $0.1K$. But they did not mention the time duration that the tubes exist stably at $0.1K$. Moreover, they explored the stability of silicon nanotubes at higher temperatures. They found that considerable structural deformations can occur when the temperature was raised to $10 - 30K$.

B. Electronic Structure

Fagan *et al* [4] [11] established theoretical similarities between silicon h-NTs and SWCNTs. Their results showed that the electronic and structural properties of silicon nanotubes are similar to those of carbon nanotubes. They found that the armchair nanotubes are metallic and all other nanotubes present an energy gap. On the other hand, Çıracı *et al* [10] analyzed more systematically the electronic structure of silicon h-NTs. Their analysis showed that zigzag single wall silicon h-NTs are metallic for $6 \leq n \leq 11$ and a band gap starts to open for $n \geq 12$. The reason for variety of results may be that different methods used.

In our studies, electronic density of states are obtained for the armchair (9,9), (10,10) and zigzag (5,0), (10,0) SW silicon h-NTs. We have shown that, depending on chiralities, as happens to carbon nanotube structures, they may present metallic or semiconducting behaviors. Figure 4.4 shows the calculated electronic density of states. We have found that the armchair nanotubes with chiralities (9,9), (10,10) are metallic and the small diameter zigzag nanotube with chirality (5,0) is semiconductor whereas the (10,0) zigzag nanotube is metallic. In Figure 4.4 the density of electronic states at the Fermi energy ($E_F = 0$) is finite for metallic (9,9), (10,10) and (10,0) nanotubes, but zero for semiconducting zigzag (5,0) nanotube. Our results are in a good agreement with the results of *ab initio* calculations by Çıracı *et al*.

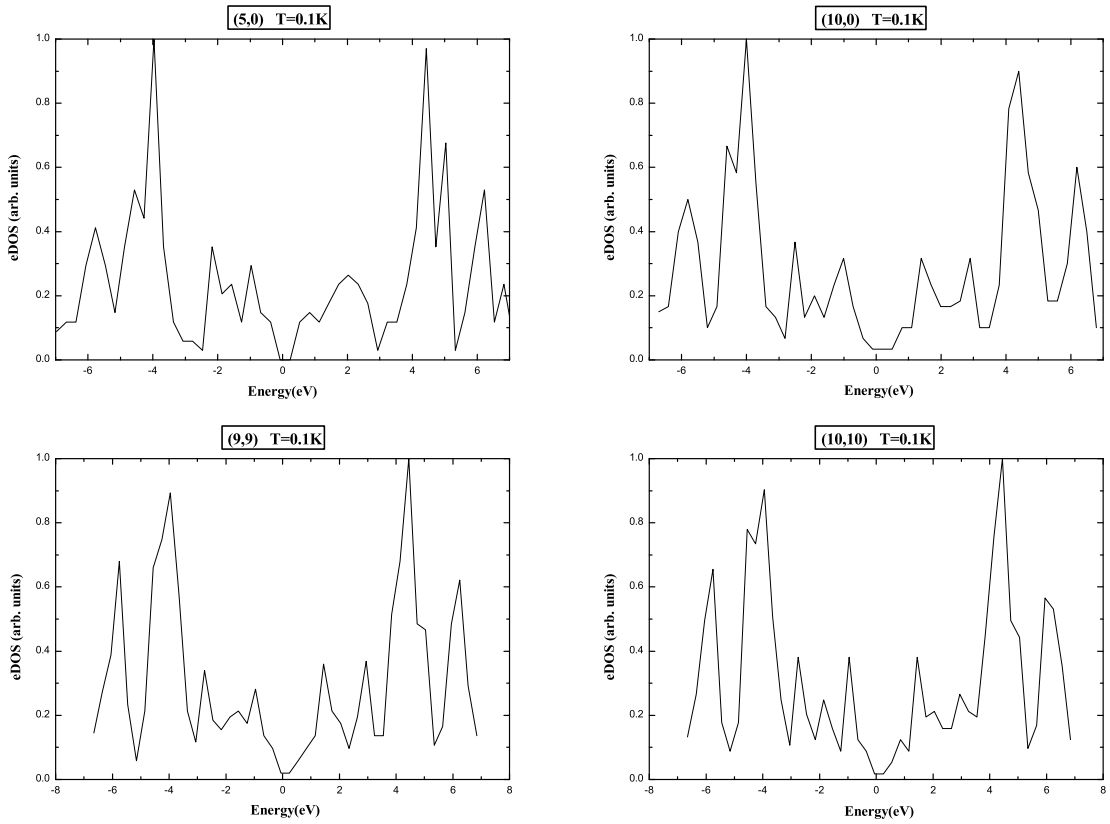

Figure 4.5: The calculated electronic density of states for the armchair (9,9), (10,10) and zigzag (5,0), (10,0) SW silicon h-NTs.

C. The Strain Energy

Dresselhaus *et al* [1] have discussed the elastic properties of SWCNTs. By rolling a graphene sheet to form a SWCNT the total energy of the tube is increased with the curvature of the nanotube. The strain energy thus increases with decreasing nanotube diameter, so that a nanotube with small diameter may be less stable than a nanotube with a larger nanotube Dresselhaus *et al.* In other words, the stability of a nanotube of particular chirality will depend on the strain energy associated with chirality.

Moreover, the energy associated with the curvature of a h-NTs should vanish in the limit as the cylindrical structure becomes a flat sheet [35]. In their study of energetics of SWCNTs, Gao *et al* [35] modeled the basic energetics of the nanotubes by approximating the nanotube as a membrane with a curvature $\frac{1}{r_t}$ and bending modulus [34] of κ. When we consider a silicon h-NT as an elastic sheet, the strain energy E_{strain} is inversely proportional to the diameter of the nanotube, r_t. Assuming h as the thickness of the sheet, from which nanotubes are formed, the strain energy per unit area is given by [35]

$$\frac{E_{strain}}{A} = \frac{\kappa h^3}{24 r_t^2} \tag{4.2}$$

and the strain energy per atom is given by

$$\frac{E_{strain}}{N} = \frac{A\kappa h^3}{N 24 r_t^2} \tag{4.3}$$

where N is the total number of atoms. Radius of curvature is also equal to the mean radius of the nanotube. Considering that the number of atoms in the nanotube wall is equal to $N = 2\pi r_t L \rho$ and the area of the sheet is $A = 2\pi r_t L$, where L is the length of the nanotube and ρ is the number density. Finally we have

$$\frac{E_{strain}}{N} = \frac{\kappa h^3}{\rho 24 r_t^2} \tag{4.4}$$

and

$$\frac{E_{total}}{N} = \frac{\kappa h^3}{\rho 24 r_t^2} + E_0 \tag{4.5}$$

where E_0 is the energy per atom for the nanotubes as $\frac{1}{r_t}$ goes to 0, i.e. flat sheets.

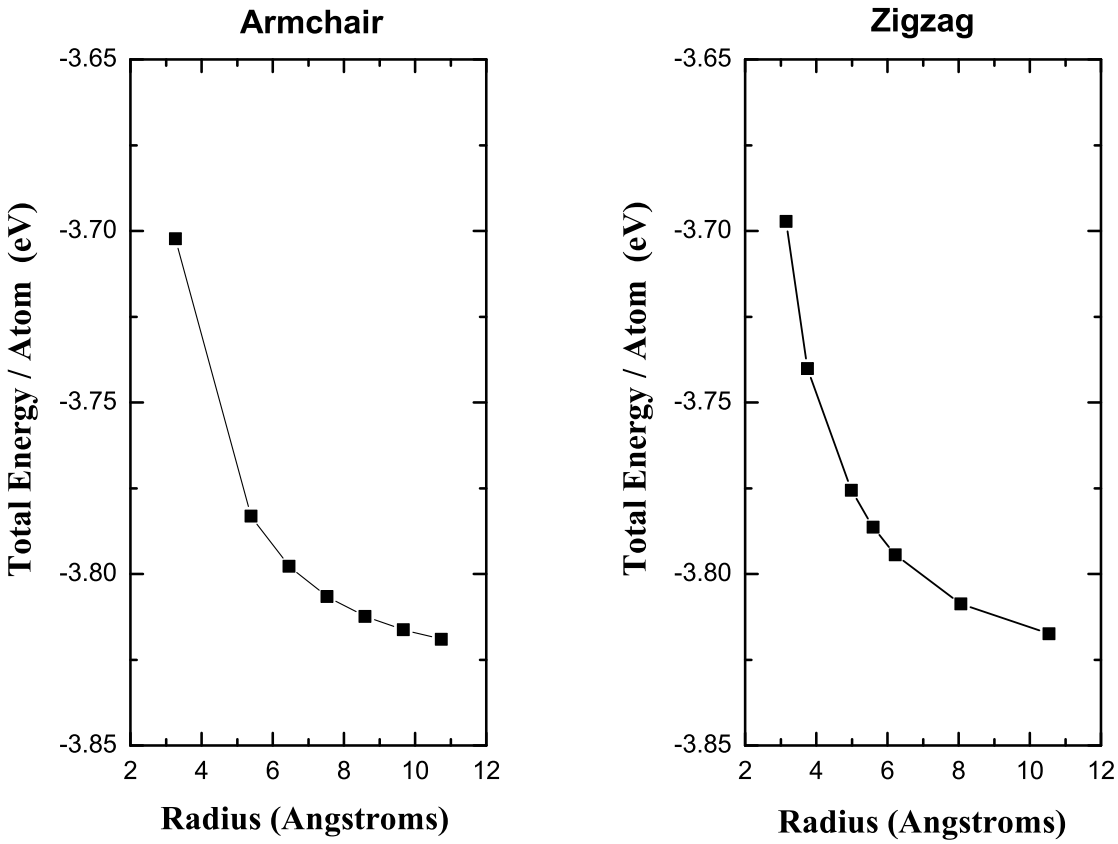

Figure 4.6: The calculated total energy (per atom) for $(n, 0)$ zigzag and (n, n) armchair single walled silicon h-NTs as a function of the nanotube diameter.

The strain energies of zigzag and armchair silicon hexagonal nanotube structures have also been obtained by Barnard *et al* [9] on the basis of DFT calculations. They have shown that we can understand the functional dependence of the strain energy of a silicon h-NT from the simple arguments given for an elastic thin film. In their studies, the argument for the dependence of strain energy per particle $\frac{E_s}{N}$ on $\frac{1}{r_t^2}$ for a silicon hexagonal nanotube is confirmed by an *ab initio* calculation of the strain energies of many zigzag and armchair h-NTs with different diameters.

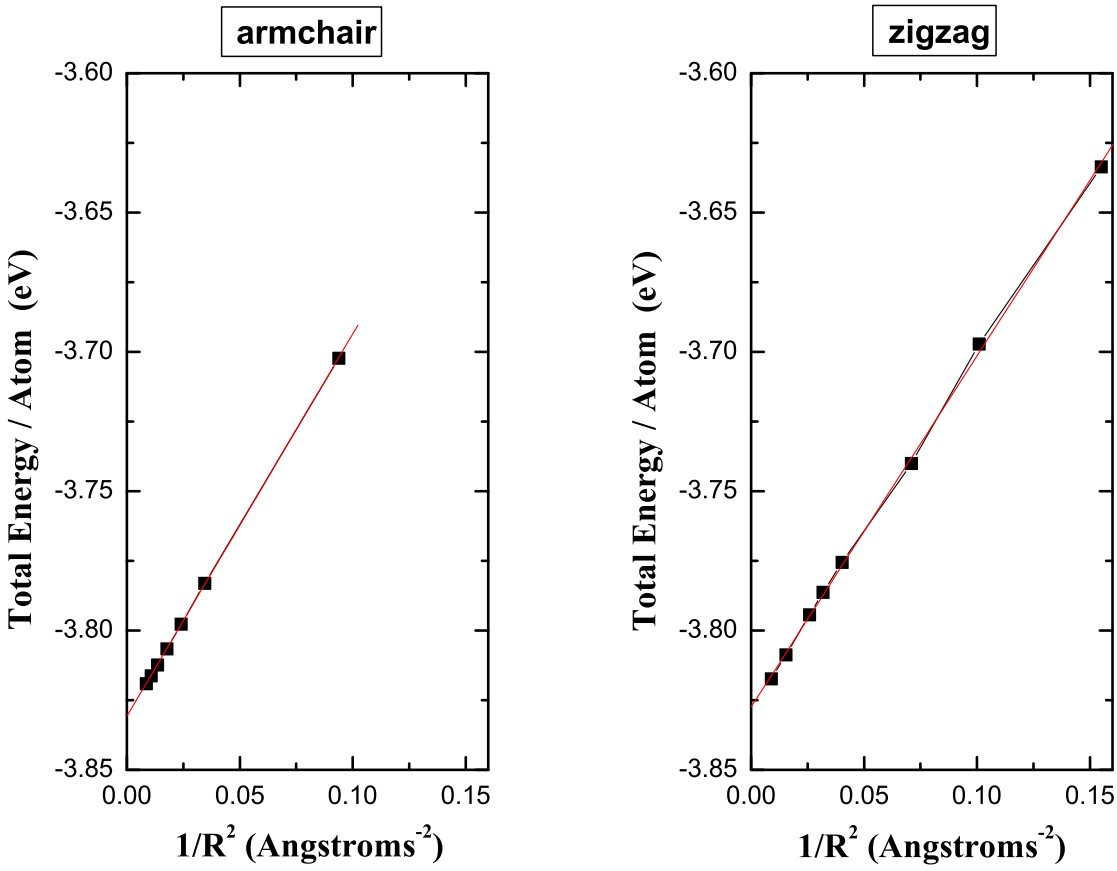

Figure 4.7: The calculated total energy (per atom) versus the inverse square of the nanotube radius for $(n, 0)$ zigzag and (n, n) armchair single walled silicon h-NTs. Linear fits are used to determine the strain energies.

In figure 4.7, we have plotted the obtained total h-NT energy (per atom) values versus $\frac{1}{r_t^2}$. Using the simple argument for an elastic thin film, from the linear fits, the intercepts give an estimate of the energy of flat graphenelike silicon sheets. We obtained graphene-like structure energy (per atom) values for the armchair and zigzag h-NT structures, as -3.8308 eV and -3.82742 eV, respectively. These results are in an agrement with the *ab initio* calculated total energy value of 3.83 eV by Fagan *et al* [4]. In addition, the slope of each fit give a value of 1.37225 eV for the armchair h-NT structure and 1.25945 eV for the zigzag structure. This result suggests the chirality dependence of the strain energy. A similar result has been obtained by Barnard *et al*, i.e. the strain energy for a zigzag (n,0) h-NT is lower than the stain energy of an armchair nanotube (n,n), for the same value of n [9].

Chapter 5

CONCLUSION

In this thesis, a systematic study about the possible stability of silicon hexagonal nanotubes (hNTs) is presented. We investigated the effects of chirality and diameter on their energetics, structural, and electronic properties. The *ab initio* structural and electronic properties of hypothetical h-NTs are given and compared with the results of our calculations.

Single walled silicon hNTs are built in analogy with SWCNTs. We studied SW silicon h-NTs using the same strategy that Dereli *et al* [18-22] developed for SWCNT TBMD simulations. Silicon hNTs are simply constructed by folding a graphenelike sheet of silicon into a cylindrical shape. Graphenelike silicon sheets are formed with the *ab initio* calculated nearest neighbor separation. Then we bent the graphenelike silicon sheet and periodic boundary conditions were imposed in axial direction along the tube and free boundary conditions in the radial direction.

First we optimized the silicon h-NTs having the same predicted total energy values reported in the literature. We obtained appropriate tight-binding potential parameters by fitting the results of *ab initio* calculations. Then starting with an initial tube structure, we considered the evolution of the system. In our calculations, electronic effects are treated in a natural way using a tight binding approximation method. A detailed explanation of the TBMD simulation techniques that we have employed is presented.

All the simulations presented in this work are carried out in the canonical (NVT) ensemble. Silicon hNTs exist stably around up to 3 ps and atoms are detached after 3 ps, according to our TBMD simulation studies. Our calculations revealed that the silicon h-NTs, formed by rolling up hexagonal graphenelike silicon structures are

metastable structures.

Predictions about the electronic properties of this material is presented. In addition, electronic properties of SWCNTs and those of silicon h-NTs are compared. Finally, we obtained strain energies of silicon h-NTs. Using the simple argument for an elastic thin film, from the linear fits, we estimated the energy of flat graphenelike silicon sheets. Moreover we showed the chirality dependence of the strain energy.

BIBLIOGRAPHY

[1] R Saito, G. Dresselhaus, M. S. Dresselhaus, *Physical Properties of Carbon Nanotubes*, Imperial College Press (1998); M. S. Dresselhaus, G. Dresselhaus, Ph. Avouris, *Carbon Nanotubes*, Springer (2001).

[2] J. W. Kang, H. J. Hwang, Nanotechnology **14**, 402 (2003).

[3] J. W. Kang, K. R. Byun, H. J. Hwang, Model. Sim. Mater. Sci. Eng. **12**, 1 (2004).

[4] S. B. Fagan, R. J. Baierle, R. Motta, J. R. Silva, A. Fazzio, Phys. Rev. B **61**, 9994 (1999).

[5] X. Yang, J. Ni, Phys. Rev. B **72**, 195426 (2005).

[6] R. Q. Zhang, H. Lee, W. Li, B. K. Teo, J. Phys. Chem. B **109**, 8605 (2005).

[7] G. G. Verri, L. C. Voon, Phys. Rev. B **76**, 075131 (2007).

[8] H. Shen, J. Mater. Sci. **42**, 6382 (2007).

[9] A. S. Barnard, S. P. Russo, J. Phys. Chem. B **107**, 7577 (2003).

[10] E. Durgun, S. Tongay, S. Çıracı, Phys. Rev. B **72**, 075420 (2005).

[11] S. B. Fagan, R. J. Baierle, R. Motta, J. R. Silva, A. Fazzio, G. Paiva, J. Molec. Str. **539**, 101 (2001).

[12] R. Q. Zhang, H. Lee, W. Li, B. K. Teo, Chem. Phys. Lett. **364**, 251 (2002).

[13] M. Zhang, Y. H. Kan, Q. J. Zang, Z. M. Su, R. S. Wang, Chem. Phys. Lett. **379**, 81 (2003).

[14] B. Yan, G. Zhou, J. Wu, W. Duan, B. Gu, Phys. Rev. B **73**, 155432 (2006).

[15] J. Sha, J. Niu, X. Ma, J. Xu, X. Zhang, Q. Yang, Adv. Mater. **73**, 1219 (2002).

[16] G. Dereli, Molec. Sim. **8**, 351 (1992).

[17] G. Dereli, M. C. Yalabık, S. Ellialtıoğlu, Phys. Scr. **40**, 117 (1989).

[18] G. Dereli, C. Özdoğan, Phys. Rev. B **67**, 035415 (2003).

[19] G. Dereli, C. Özdoğan, T. Çağın, Comp. Phys. Comm. **148**, 188 (2002).

[20] G. Dereli, C. Özdoğan, Phys. Rev. B **67**, 035416 (2003).

[21] G. Dereli, B. Süngü, C. Özdoğan, Nanotechnology **18**, 245704 (2007).

[22] G. Dereli, B. Süngü, Phys. Rev. B **75**, 184104 (2007).

[23] C. H. Xu, C. Z. Wang, C. T. Chan, K. M. Ho, J. Phys. Condens. Matter **4**, 6047 (1992).

[24] I. Kwon, R. Biswas, C. Z. Wang, K. M. Ho, C. M. Saukolis, Phys. Rev. B **49**, 7242 (1994).

[25] L. Colombo, Comp. Mat. Sci. **12**, 278 (1998).

[26] L. Colombo, M. Rosati, Comp. Phys. Comm. **108**, 128 (2000).

[27] L. Goodwin, A. J. Skinner, D. G. Pettifor, Europhys. Lett. **9**, 701 (1989).

[28] R. Virkkunen, K. Laasonen, R. M. Nieminen, J. Phys. Condens. Matter **3**, 7455 (1991).

[29] R. Car, M. Parrinello, Phys. Rev. Lett. **60**, 204 (1988).

[30] See, for example, N. W. Ashcroft, N. D. Mermin, *Solid State Physics*, International Thomson Publishing (1976).

[31] See, for example, M. P. Allen, D. J. Tildesley, *Computer Simulation of Liquids*, Oxford University Press (1996).

[32] See, for example, J. J. Sakurai, *Modern Quantum Mechanics*, Addison-Wesley (1994).

[33] See, for example, J. Z. Zhang, *Theory and Application of Quantum Molecular Dynamics*, World Scientific Publishing (1999).

[34] L. D. Landau, E. M. Lifshitz, *Theory of Elasticity*, Pergamon Press (1970).

[35] G. Gao, T. Çağın, W. A. Goddard, Nanotechnology **9**, 184 (1998).

VITA

MUSTAFA SELÇUK YAŞAR was born in Ankara, Turkey on January 14, 1982. He received his B.Sc. degree in Physics from Koç University, Istanbul, Turkey in June 2006. In August 2006, he was accepted to Master of Science in Physics programme at Koç University with full scholarship. From August 2006 to August 2008, he worked as a teaching assistant in Koç University. He has studied on properties of carbon and silicon nanotubes using tight-binding molecular dynamics simulation techniques. He studied for the *"Molecular Dynamics Simulation Study of Silicon Nanotubes"* project with Prof. Tekin Dereli and Prof. Gülay Dereli.